Biochemical Pharmacology 199 (2022) 115023

Contents lists available at ScienceDirect

Biochemical Pharmacology

journal homepage: www.elsevier.com/locate/biochempharm

sVmKTx, a transcriptome analysis-based synthetic peptide analogue of Vm24, inhibits Kv1.3 channels of human T cells with improved selectivity

Agota Csoti [a], Rosby del Carmen Nájera Meza [b], Ferenc Bogár [c,d], Gabor Tajti [a], Tibor G. Szanto [a], Zoltan Varga [a], Georgina B. Gurrola [b], Gábor K. Tóth [c,d], Lourival D. Possani [b], Gyorgy Panyi [a,*]

[a] Department of Biophysics and Cell Biology, Faculty of Medicine, Research Center for Molecular Medicine, University of Debrecen, 1 Egyetem ter, Debrecen 4032, Hungary
[b] Departamento de Medicina Molecular y Bioprocesos, Instituto de Biotecnología, Universidad Nacional Autonoma de Mexico, Avenida Universidad, 2001, Cuernavaca, Morelos 62210, Mexico
[c] Department of Medical Chemistry, Albert Szent-Györgyi Medical School, University of Szeged, 6720 Szeged, Dóm tér 8, Hungary
[d] MTA-SZTE Biomimetic Systems Research Group, Eötvös Loránd Research Network (ELKH), University of Szeged, 6720 Szeged, Dóm tér 8, Hungary

ARTICLE INFO

Keywords:
Kv1.3
Scorpion toxin
Ion channel selectivity
Patch-clamp
T-cell activation
Toxin-channel interaction

ABSTRACT

Kv1.3 K^+ channels play a central role in the regulation of T cell activation and Ca^{2+} signaling under physiological and pathophysiological conditions. Peptide toxins targeting Kv1.3 have a significant therapeutic potential in the treatment of autoimmune diseases; thus, the discovery of new toxins is highly motivated. Based on the transcriptome analysis of the venom gland of *V. mexicanus smithi* a novel synthetic peptide, sVmKTx was generated, containing 36 amino acid residues. sVmKTx shows high sequence similarity to Vm24, a previously characterized peptide from the same species, but contains a Glu at position 32 as opposed to Lys32 in Vm24. Vm24 inhibits Kv1.3 with high affinity (K_d = 2.9 pM). However, it has limited selectivity (~1,500-fold) for Kv1.3 over hKv1.2, hKCa3.1, and mKv1.1. sVmKTx displays reduced Kv1.3 affinity (K_d = 770 pM) but increased selectivity for Kv1.3 over hKv1.2 (~9,000-fold) as compared to Vm24, other channels tested in the panel (hKCa3.1, hKv1.1, hKv1.4, hKv1.5, rKv2.1, hKv11.1, hKCa1.1, hNav1.5) were practically insensitive to the toxin at 2.5 μM. Molecular dynamics simulations showed that introduction of a Glu instead of Lys at position 32 led to a decreased structural fluctuation of the N-terminal segment of sVmKTx, which may explain its increased selectivity for Kv1.3. sVmKTx at 100 nM concentration decreased the expression level of the Ca^{2+} -dependent T cell activation marker, CD40 ligand. The high affinity block of Kv1.3 and increased selectivity over the natural peptide makes sVmKTx a potential candidate for Kv1.3 blockade-mediated treatment of autoimmune diseases.

1. Introduction

Scorpion venoms consist of complex mixtures of hundreds of different proteins and other molecules, some of which have enzymatic and cytolytic activities and thus harmful effects on humans [1,2]. However, venoms also contain molecules with potential therapeutic effects. Of these, the ones targeting ion channels in the plasma membrane, such as voltage-gated K^+, Na^+ and Ca^{2+} channels, Ca^{2+}-activated K^+ channels and Cl^- channels, or in the cytosol, such as Ryanodine receptor, have paramount importance [3–9]. There are over 200 scorpion toxins in 7 subfamilies (α, β, γ, δ, ε, κ, and λ) that target voltage-gated K^+ channels, of these the α family (α-KTx) being the largest containing ~150 members. α-KTx share a common structural motif, called cysteine-stabilized α/β scaffold (CS-αβ), in which the α-helix is connected to at least two β-sheets by 3–4 disulfide bridges [10,11].

The classical methods of peptide identification, that include chromatographic separation combined with mass spectrometry or Edman degradation, led to the discovery of a large number of peptides [12].

Abbreviations: EGTA, ethylene glycol-bis(β-aminoethyl ether)-N,N,N′,N′-tetraacetic acid; HEPES, 4-(2-hydroxyethyl)-1-piperazineethanesulfonic acid; MD, molecular dynamics; MM-GBSA, molecular mechanics-generalized Born surface area; RCF, remaining current fraction; RMSF, root-mean-squared fluctuations; sVmKTx, synthetic mature peptide of GenBank accession number JZ818447.1; T_{EM}, effector memory T cell; TFA, trifluoroacetic acid; Vm24, peptide isolated from *Vaejovis mexicanus,* α-KTx 23.1, 2K9O.

* Corresponding author at: Department of Biophysics and Cell Biology, Faculty of Medicine, Research Center for Molecular Medicine, University of Debrecen, 1 Egyetem ter, Debrecen 4032, Hungary.
E-mail address: panyi@med.unideb.hu (G. Panyi).

https://doi.org/10.1016/j.bcp.2022.115023
Received 7 February 2022; Received in revised form 22 March 2022; Accepted 23 March 2022
Available online 28 March 2022

Later the new approach was the Edman degradation peptide sequencing complementation [13]. One of the major limitations of this approach is the purification and isolation of sometimes miniature quantities of the toxins in the venom. To overcome this limitation venom gland transcriptome analysis has been introduced recently resulting in the discovery of several novel peptides [14–16]. For example, the transcriptome analysis of *Vaejovis mexicanus* permitted the identification the total of 197 express sequence tags (ESTs), of which of 23 (11.7%) have sequence similarities to toxins [17]. The predictions regarding the biological activity of these peptides, however, must be confirmed with electrophysiology using recombinantly or synthetically produced peptides. The combination of these techniques allows for pharmacological characterization or structural determination of the peptides predicted to exist based on the venom transcriptome.

Among the peptide toxins targeting Kv channels, the identification and characterization of Kv1.3 inhibitor peptides bear great significance due to their potential therapeutic application in the management of Kv1.3-dependent immunological diseases [18]. Chronically activated effector memory T lymphocytes (T_{EM}) play an important role in the pathogenesis of autoimmune diseases such as multiple sclerosis, type 1 diabetes mellitus or rheumatoid arthritis [19,20]. These T cells are characterized by high Kv1.3 expression, thus their proliferation can be suppressed, and the symptoms of experimental autoimmune disease could be ameliorated by Kv1.3 inhibitors. The molecular mechanism behind this effect is that Kv1.3 maintains a permissive membrane potential for efficient Ca^{2+} signaling through the Ca^{2+}-release activated Ca^{2+} channels in T cells. Kv1.3 inhibitors depolarize T cells and in turn, diminish the driving force for Ca^{2+} entry into the cells upon T cell activation [21–23]. Thus, Kv1.3 is an important pharmacological target for treating autoimmune diseases [18].

Several peptide toxins have been isolated and characterized as high affinity blockers of the Kv1.3 ion channel [5,24]. Among these, Vm24 (α-KTx 23.1) is a 36-residue Kv1.3-blocker peptide from the venom of the scorpion *Vaejovis mexicanus smithi*. Vm24 blocks Kv1.3 channel with high affinity (K_d = 2.9 pM) and displays excellent, over ~1500-fold Kv1.3 selectivity against several ion channels. However, at high peptide concentrations (over 10 nM) it also blocks other ion channels including Kv1.1, Kv1.2 and KCa3.1 [25]. The transcriptome analysis of *V. mexicanus smithi* identified a 36-residue peptide with high sequence similarity to Vm24. The difference between the two toxins is one amino acid residue: Vm24 contains a positively charged lysine at position 32 whereas the novel peptide contains a negatively charged glutamate at the identical position [17].

In this study we synthetically produced this novel peptide referred to as sVmKTx and investigated whether the unique similarity of sVmKTx with Vm24 is reflected in its pharmacological properties. sVmKTx blocked Kv1.3 channels with high, albeit decreased affinity (K_d = 770 pM) as compared to Vm24. This change in the potency was associated with higher selectivity for Kv1.3 than Vm24 against a panel of channels used in this study (hKv1.3 ≫ hKv1.2 ≫ hKCa3.1 ≈ hKv1.1 ≈ hKv1.4 ≈ hKv1.5 ≈ rKv2.1 ≈ hKv11.1 ≈ hKCa1.1 ≈ hNav1.5). Molecular mechanics-generalized Born surface area (MM-GBSA) binding free energy calculations reported that the Lys32Glu substitution weakened the binding of sVmKTx to His451 residues in two subunits of the Kv1.3 tetramer. Molecular dynamics simulations showed that the Lys32Glu substitution led to a decreased structural fluctuation of the N-terminal segment of sVmKTx, which may explain its increased selectivity for Kv1.3. Adding 100 nM sVmKTx to T cells decreased the expression level of CD40 ligand, which is an early, Ca^{2+} -dependent T cell activation marker. The high affinity block of Kv1.3 and increased selectivity over the natural peptide makes sVmKTx a potential candidate for Kv1.3 blockade-mediated treatment of autoimmune diseases, in which the T_{EM} cells play an important role.

2. Materials and methods

2.1. sVmKTx production and chemical characterization

A linear analogue of sVmKTx was synthesized by a solid phase methodology on rink amide MBHA resin (Calbiochem- Novabiochem Corp., San Diego, CA). Fmoc-amino acids (Calbiochem-Novabiochem Corp.) were used with the following side chain protection: Arg(Pbf), Asn (Trt), Cys(Trt), Gln(Trt), Glu(OtBu), Lys(Boc), Ser(tBu), and Tyr(tBu). The Fmoc group was removed by treatment with 20% piperidine in dimethylformamide (DMF) for 20 min followed by a wash with DMF. Fmoc- amino acids (0.2 mmol) were coupled as active esters, which was performed in DMF with HBTU [2-(1H- benzotriazol-1-yl)-1,1,3,3-tetramethyluronium hexafluorophos-phate]. HOBt (N-Hydroxybenzotriazole) and DIEA (diisopropylethylamine) (0.175, 0.172 and 0.3 mmol, respectively; activation for 2 min) as activating agents. Coupling times were 2 hrs. Unreacted or deblocked free amines were monitored through the ninhydrin test in every cycle of the peptide synthesis [26]. During the entire synthesis, before the next amino acid was coupled, the undesirable residual free amines were blocked by acetylation. All the operations were performed manually in a 20 ml glass reaction vessel with a Teflon-lined screw cap. The peptide resin was agitated by gentle inversion during the Nα-deprotection and coupling steps.

Following final removal of the Fmoc group, the peptide resin (150 mg) was cleaved from the resin and simultaneously deprotected using 10 ml of reagent K (84% TFA (trifluoroacetic acid), 5% Phenol, 5% Thioanisole, 5% H_2O, 1% DTT (dithiothreitol)) for 2 h at room temperature. Following cleavage, the crude peptide was precipitated and washed with ice-cold *tert*-butyl ether and then dissolved in 20% aqueous acetic acid. The product was lyophilized and kept desiccated at −20 °C until it was used.

The cyclization reaction to make the corresponding disulfide bridges of the molecule was conducted in 0.1 M NaCl, 5 mM reduced glutathione, 0.5 mM oxidized glutathione, 20 mM Na_2HPO_4 (pH 7.8), and 0.1 mg/ml unfolded synthetic VmKTx. The crude cyclized product was purified in two steps by HPLC. The first used a C18 preparative column (238TP1022 Vydac, Grace Corp., Columbia, MD.), with a linear gradient of solution A (0.12% TFA in water) to solution B (0.1% TFA in acetonitrile) run up to 60% B over 60 min. The main component was further separated as described under Results.

The homogeneity of the peptide was verified by mass spectrometry (only one component) and by Edman degradation procedure. Mass spectrometry analysis was conducted in a LCQFleet apparatus from Thermo Fisher Scientific Inc. (San Jose, CA, USA) and the amino acid sequence determination by Edman degradation was performed using a Shimadzu Protein Sequencer PPSQ-31A/33A (Columbia, Maryland, USA) as described elsewhere [26].

2.2. Human T lymphocytes for patch-clamp recordings

Heparinized human peripheral venous blood was obtained from healthy volunteers. Mononuclear cells were separated through Histopaque-1077 (Sigma-Aldrich Hungary, Budapest, Hungary) density gradient centrifugation. Collected cells were washed twice with Ca^{2+}- and Mg^{+}-free Hanks' solution containing 25 mM HEPES buffer, pH 7.4. Cells were cultured for 2–5 days in 24-well culture plates in a 5% CO_2 incubator at 37 °C, in RPMI 1640 medium supplemented with 10% fetal calf serum (Sigma-Aldrich), 100 μg/ml penicillin, 100 μg/ml streptomycin, and 2 mM L-glutamine (density, 0.5 × 10^6 cells per ml). The culture medium also contained 6 or 12 μg/ml phytohemagglutinin A (Sigma-Aldrich), to increase K^+ channel expression. Cells were washed gently twice with 5 ml of normal extracellular bath medium (see below) for the patch-clamp experiments.

2.3. Human T cells for CD40L staining; T cell activation

Buffy coats from anonymized healthy donors were obtained from blood bank donors. Mononuclear cells were separated through density gradient centrifugation, using Histopaque-1077 (Sigma-Aldrich, Budapest, Hungary). $CD4^+$ T lymphocytes were purified by magnetic-activated cell sorting (positive selection) with the REAlease® $CD4^+$ MicroBead Kit (Miltenyi Biotec GmbH, Bergisch Gladbach, Germany) [27]. Dead cells were removed using the Dead Cell Removal Kit (Miltenyi Biotec GmbH, Bergisch Gladbach, Germany). Cells were cultured in 96-well plates (200,000/well) in 5% CO_2 incubator at 37 °C, in RPMI-1640 medium supplemented with 10% fetal bovine serum (Sigma-Aldrich), 100 μg/ml penicillin, 100 μg/ml streptomycin, and 2 mM L-glutamine. $CD4^+$ T lymphocytes were divided into three groups: 1. unstimulated cells, 2. stimulated cells, 3. stimulated cells + sVmKTx (100 nM). For TCR-specific stimulation DynaBeads Human T-Activator αCD3/αCD28 for T Cell Expansion and Activation (Thermo Fischer Scientific, Budapest, Hungary) was used according to the manufacturer's protocol. For group 3, cells were pre-incubated with the sVmKTx toxin (100 nM) for five minutes before activation. Cells were incubated at 37 °C in 5% CO_2 for the indicated times. To determine the optimal length of activation, in which the IL-2 production and the consequent auto-activation of the cells can be avoided, activated cells were sampled and analyzed by cell surface staining of CD40L at different time points (see results).

2.4. Measurement of CD40L surface expression

To quantify T-cell activation, CD40L surface expression was determined accordingly: cells were resuspended in 100 μl of phosphate-buffered saline supplemented with 1% fetal bovine serum and were incubated with fluorescein isothiocyanate (FITC) -labeled anti-CD40L (BioLegend Inc., San Diego, CA) for 30 min at 4 °C according to the manufacturers protocol. Cells were then washed with phosphate-buffered saline, centrifuged at 400*g* and were fixed in 2% para-formaldehyde. Samples were measured with NovoCyte Flow Cytometer system (ACEA Bioscience Inc., Santa Clara, CA, USA) and were analyzed with FCS Express 6.0 (De Novo Software, Glendale, CA). After FSC-SSC gating, CD40L expression was analyzed. Negative (unlabeled) and non-stimulated controls were always prepared and assessed for comparison.

2.5. Ethical statement

The use of human T cells for electrophysiology was approved by the Ethical Committee of the Hungarian Medical Research Council (36255-6/2017/EKU). Informed consent was obtained from each participant. The investigation conforms to the principles outlined in the Declaration of Helsinki.

2.6. Cells for heterologous expression of ion channels

Human embryonic kidney 293, CHO and MEL cells were grown under standard conditions, as described previously [28–30].

2.7. Expression of recombinant ion channels

CHO cells were used to express hKv1.1 (in pCMV6-GFP plasmid OriGene Technologies, Rockville, MD), hKv1.2 (in pCMV6-GFP plasmid OriGene Technologies, Rockville, MD), hKv1.4 (hKv1.4-IR, the inactivation ball deletion mutant of Kv1.4; a kind gift from D. Fedida, University of British Columbia, Vancouver, Canada), rKv2.1 (a kind gift from Dr. S. Korn, University of Connecticut, Storrs, CT), hKCa1.1 (hSlo1 gene in pCI-neo plasmid, GenBank accession no. U11058; a gift from T. Hoshi, University of Pennsylvania, Philadelphia, PA), and hNav1.5 (a gift from R. Horn, Thomas Jefferson University, Philadelphia, PA). These channel clones were transiently co-transfected with a plasmid encoding the green fluorescent protein (GFP) (except for hKv1.1 and hKv1.2 where GFP-tagged ion channel vectors were used), at molar ratios of 1:5, by using Lipofectamine 2000 (Invitrogen, Thermo Fischer Scientific, Budapest, Hungary) according to the manufacturer's protocol and were cultured under standard conditions. Currents were recorded 24 h after transfection. GFP-positive transfectants were identified with a Nikon Eclipse TS100 fluorescence microscope (Nikon, Tokyo, Japan) and were used for current recordings (>70% success rate for co-transfection). MEL cells stably expressing the hKv1.5 channel [30] and CHO cells stably expressing the hKCa3.1 channel and were gifts from Dr. Heike Wulff (University of California, Davis, CA, USA), hKv11.1 (hERG) channels were expressed in a stable manner in HEK 293 cells.

2.8. Electrophysiological experiments

Whole-cell currents were measured in voltage-clamped cells according to standard protocols [25,28,29,31], using a Multiclamp 700B amplifier connected to a personal computer with Axon Digidata 1440A data acquisition hardware (Molecular Devices, Sunnyvale, CA). Series resistance compensation up to 70% was used to minimize voltage errors and to achieve good voltage-clamp conditions. Cells were observed with Nikon Eclipse TS100 (Nikon, Tokyo, Japan) fluorescence microscope, by using band-pass filters of 455–495 nm and 515–555 nm for excitation and emission, respectively. Cells displaying strong fluorescence were selected for current recordings, and >70% of those cells displayed co-transfected current. Pipettes were pulled from GC 150F-15 borosilicate glass capillaries Harvard Apparatus (Kent, UK) in five stages and fire-polished, which resulted in electrodes having 3–5-MΩ resistance in the bath. Solutions: all salts and solution components were purchased from Sigma-Aldrich, Budapest, Hungary. For measurements of most channels, the bath solution consisted of 145 mM NaCl, 5 mM KCl, 1 mM $MgCl_2$, 2.5 mM $CaCl_2$, 5.5 mM glucose, and 10 mM HEPES, pH 7.35, supplemented with 0.1 mg/ml bovine serum albumin. For recordings of hKv11.1 (hERG) currents, the bath solution contained 140 mM choline chloride, 5 mM KCl, 2 mM $MgCl_2$, 2 mM $CaCl_2$, 0.1 mM $CdCl_2$, 20 mM glucose, and 10 mM HEPES (pH 7.35). hKCa3.1 currents were recorded with an external solution of the following composition: 160 mM L-aspartic acid (Na^+ salt), 5 mM KCl, 2.5 mM $CaCl_2$, 1 mM $MgCl_2$ and 10 mM HEPES, pH 7.4. The measured osmolarity of the external solutions was between 302 and 308 mOsM. The internal solution contained 140 mM KF, 2 mM $MgCl_2$, 1 mM $CaCl_2$, 10 mM HEPES, and 11 mM EGTA (pH 7.22). For recordings of hKCa1.1 (hBK) currents, the composition of the pipette filling solution was 140 mM KCl, 10 mM EGTA, 9.69 mM $CaCl_2$, 5 mM HEPES, pH 7.2. The free Ca^{2+} concentration of the latter solution was 5 μM, which allowed recording of hKCa1.1 currents at moderately depolarizing potentials [32]. For recordings of KCa3.1 currents, the composition of the pipette filling solution was 150 mM potassium aspartate, 5 mM HEPES, 10 mM EGTA, 8.7 mM $CaCl_2$, 2 mM $MgCl_2$, pH 7.2. This solution contained 1 μM free Ca^{2+}, to activate the KCa3.1 current fully [33]. For recordings of Kv11.1 currents, the pipette solution contained 140 mM KCl, 10 mM EGTA, 2 mM $MgCl_2$, and 10 mM HEPES, pH 7.3. For recordings of Nav1.5 currents, the composition of the pipette filling solution was 105 mM CsF, 10 mM NaCl, 10 mM EGTA and 10 mM HEPES, pH 7.2. The measured osmolarity of the internal solutions was approximately 295 mOsM. Bath perfusion around the measured cell with different test solutions was achieved by using a gravity-flow perfusion system. Excess fluid was removed continuously. For measurements of currents from hKv1.1, hKv1.2, hKv1.3, fast inactivation-removed hKv1.4 (Kv1.4ΔN), hKv1.5, and rKv2.1 channels, voltage steps to +50 mV were applied from a holding potential of –120 mV every 15 or 30 s. For hKv11.1 (hERG) channels, currents were evoked with a voltage step to +20 mV followed by a step to –40 mV, during which the peak current was measured. The holding potential was –80 mV, and pulses were delivered every 30 s. For KCa1.1 channels, a voltage step to +50 mV was preceded by a 50-ms hyperpolarization to –100 mV from a holding potential of –120 mV. Pulses were delivered

every 15 s. hKCa3.1 currents were elicited every 15 s with voltage ramps to +50 mV from a holding potential of –120 mV. Currents through Nav1.5 channels were evoked every 15 s with voltage steps to 0 mV from a holding potential of –120 mV. For data acquisition and analysis, the pClamp10 software package (Molecular Devices, Sunnyvale, CA) was used. In general, currents were lowpass- filtered by using the built-in analog four-pole Bessel filters of the amplifiers and were sampled (2–50 kHz) at least twice the filter cut-off frequency. Before analysis, whole-cell current traces were corrected for ohmic leakage and were digitally filtered (three-point boxcar smoothing). Each data point of the concentration–response curves represents the mean of three to six independent experiments, and error bars represent the SEM. Data points were fitted with a two-parameter Hill equation, $RCF = K_d^H/(K_d^H + [Tx]^H)$, where RCF is the remaining current fraction ($RCF = I/I_0$, where I and I_0 are current amplitudes in the presence and absence, respectively, of toxin at a given concentration), K_d is the dissociation constant, H is the Hill coefficient, and [Tx] is the toxin concentration. Where indicated, K_d was estimated from the RCF value obtained with a single toxin concentration assuming $H = 1$.

2.9. Statistical analysis

All data are presented as means ± SEM. Statistical analysis were using Student's *t*-test (unpaired). Statistical analysis was performed using GraphPad v.8. (GraphPad Software LLC, San Diego, CA, USA).

2.10. 3D structure of sVmKTx

As sequence of sVmKTx differs from Vm24 only in one amino acid residue (K32E), we used the previously published NMR structure of the latter peptide (Protein Data Bank ID: 2K9O) [26] as initial guess to generate the 3D structure of the investigated sVmKTx toxin. Twenty slightly different conformers of Vm24 can be found in PDB file 2K9O. These structures were grouped to five clusters using the conformation clustering tool of the Schrödinger package (Schrödinger Release 2019-4. Schrödinger, LLC, New York, NY). Representative structures (the closest one to the average structure) of these clusters were used in our computational stability and docking investigations. The K32E mutants were generated from these structures with the help of the residue scanning tool of the Schrödinger package.

2.11. Homology model of the human Kv1.3 ion channel

The amino acid sequence of human Kv1.3 channel was taken from the Uniprot database (ID P22001). The homology model was created only for the inner region of the channel, namely amino acid residues 383–491 using the original Uniprot numbering. The X-ray structure of ChTx bound Kv1.2-2.1 chimera ion channel (*Rattus Norvegicus*, PDB ID: 4JTA) [34] was used as a template. hKv1.3 has as high sequence identity as 93% in the selected region (see results). Homology model of human Kv1.3 ion channel was created with the Prime program from the Schrödinger package, and it was refined using the Protein Preparation Wizard of the same package.

2.12. ToxDock protocol to Rosetta

ToxDock protocol is a combination of ensemble-docking and extensive conformational sampling. It was successfully applied for docking α-GID and its analogs to an α4β2 nAChR homology model [35]. The same protocol was used to find the best docking poses of Vm24 and sVmKTx to the homology model of human Kv1.3 channel. Five were selected from the NMR based experimental structures of Vm24 [26] and fitted to the ChTx structure providing initial structures for the docking. The results were collected and 5 structures with the highest surface interaction were selected from the 25 highest ranked docking poses for further molecular dynamical investigations. The same procedure was applied to the sVmKTx toxin using the K32E mutant structures.

2.13. Conformational sampling of Vm24 and sVmKTx and their complex with hKv1.3 ion channel

Structural differences of sVmKTx and Vm24 were investigated using an extended conformational sampling method, the replica exchange solute tempering (REST) molecular dynamics (MD) [36,37] as it is implemented in the Desmond code (Schrödinger Release 2019-4, Schrödinger, LLC, New York, NY). The toxins were centered in orthorhombic boxes filled with water molecules and NaCl in 0.15 M final concentration. The charges of the toxins were neutralized with additional Cl^- ions. The shortest distance between the toxin and the walls of the box was 10 Å. The OPLS3e force-field [38] was applied for the toxins, water molecules were parametrized using the SPC (simple point-charge) water model. The initial structure was relaxed before the production run using the following five-step protocol: (1) 100-ps-long Brownian NVT dynamics at 10 K with 1 fs time steps and restraints on solute heavy atoms, (2) 12-ps-long NVT dynamics at 10 K with 1 fs time steps and the same restraint, (3) 12-ps-long NPT dynamics at 10 K with 1 fs time steps retaining the restraint, (4) 12-ps-long NPT dynamics at 300 K with 2 fs time steps with restraints on solute heavy atoms, and finally, (5) 24-ps-long molecular dynamics calculation of the same kind was carried out without any restraints. Six simultaneous 200 ns-long NPT molecular dynamics calculations at different temperatures between 300 K and 390 K were carried out to collect representative conformational samples of the investigated toxins at these temperatures. For the parameters not described here we used the default settings of the Desmond program. The last 100 ns of the 300 K replica of the REST simulation was selected to characterize the structural differences of sVmKTx and Vm24. To this end, root-mean-squared fluctuations (RMSF) of the non-H atoms of the amino acid residues and H-bond analysis of K32 and E32 residues with the remaining part of the toxins were carried out with the corresponding utilities from the Schrödinger package (Schrödinger Release 2019-4. Schrödinger, LLC, New York, NY).

The binding modes of sVmKTx and Vm24 to the hKv1.3 ion channel were compared using molecular dynamics based conformational samplings started from the best docking poses obtained with the ToxDock protocol described above. Five independent 100-ns-long NPT MD simulations with the OPLS3e force-field [38] and the SPC water model was completed for both toxin-ion-channel complexes. The parameters of the simulation as well as the relaxation steps used for the initial structures were the same as it is described at REST simulation above. Cumulated trajectory points collected from the last 50 ns of these calculations were used in MM-GBSA residue interaction mapping.

2.14. MM-GBSA binding pattern analysis

Binding affinities (ΔG) of toxins were calculated using the molecular mechanics-generalized Born surface area (MM-GBSA) approximation, which was originally developed for ligand-receptor complexes and was successfully applied in several molecular design studies [39–41].

In this method the estimated binding free energy of a ligand (ΔG) is calculated using the single trajectory approach [42], in which a single MD simulation of the protein–ligand complex is carried out providing regular conformational samples of the complex. For each structure

$$\Delta G = G_{PL} - G_P - G_L$$

was calculated, where G_{PL}, G_P and G_L are the energy of the protein ligand complex, protein and ligand in a geometry obtained from the MD trajectory points. These energy values are calculated as

$$G = G_{MM} + G_{Solv},$$

where G_{MM} is the calculated molecular mechanics energy for the force field applied, and G_{Solv} is the solvation energy in the generalized Born

name	sequence	n	%I
Vm24	AAAISCVGSPECPPKCRAQGCKNG***K***CMNRKCKC***Y***YC	36	100
sVmKTx	AAAISCVGSPECPPKCRAQGCKNG***K***CMNRKCEC***Y***YC	36	97.2
	********************************:****		

Fig. 1. Alignment of the sVmKTx sequence with Vm24. The percentage of identity (% I) was determined with LALIGN v. 2.1.30. The alignments were performed with CLUSTALX v. 2.0. (*) shows conserved amino acids and (:) the variable amino acids. The number of amino acid residues is indicated by n. Amino acids indicated by bold italic are the diad amino acids essential for Kv channel inhibition. The accession number for Vm24 in the UniProtKB is P0DJ31.

approximation. Different variations of this method are widely used in large scale drug design studies (for a recent review see [43]) although doubts also emerged considering its accuracy [44]. In addition to the absolute binding free energy, MM-GBSA method is also applicable in identification of the critical interactions for rational drug design. For this purpose, the total binding free energy of a ligand is decomposed to per-residue contributions. This way the interaction pattern of the investigated compounds can be quantitatively compared residue by residue [45].

Standard error of mean (SEM) of total binding free energy as well as its per-residue contributions were calculated with the help of bootstrap error estimation following the work of Aldeghi et al. [46]. A total of 10^5 samples were generated using random resampling with replacement of the calculated binding free energy values, and the standard deviation of the resulting distribution of the means was taken as error estimation.

The actual calculations were carried out with the thermal_mmgbsa.py script of the Schrödinger package from the evenly spaced 100 structures of the last 50 ns of each of the five production MD simulations executed for both toxin-protein complexes.

3. Results

3.1. Production and structural characterization of sVmKTx

During the transcriptome analysis of the venomous gland of the scorpion *Vaejovis mexicanus* a very similar peptide to Vm24 toxin was identified [17] and named as VmKTx1 (GenBank accession number in JZ818447.1). To verify the function of VmKTx1 chemical synthesis of the predicted peptide was performed and was referred to as sVmKTx thereafter. Fig. 1 shows the predicted mature peptide containing 36 amino acid residues and a multiple alignment between the known primary sequence of Vm24 and the synthetic peptide sVmKTx. The only difference between the two peptides is in position 32, where a glutamic acid substitutes for a lysine found in Vm24.

After synthesis and folding the peptide was purified by two consecutives HPLC separations. The final purification profile is shown in Fig. 2A. The principal component (main peak, without the small lateral shoulder) was selected for this work. This component was homogeneous as shown by Edman degradation. The molecular mass determined by mass spectrometry was 3865.75 Da, showing that it corresponds exactly to that of the expected sequence (Fig. 2B). It is worth noting that the resin used is designed to produce a C-terminally amidated peptide, exactly like the case for native Vm24.

3.2. sVmKTx is a high-affinity, reversible blocker of hKv1.3 channels

The standard voltage protocol used to evoke voltage-gated, hKv1.3-mediated, K^+ currents in T cells consisted of a series of 15-ms depolarizations from a holding potential of –120 mV to +50 mV (to maximize the open probability of the channel). The time between voltage pulses was set to 15 s, to avoid cumulative inactivation of hKv1.3 channels. Under the experimental conditions applied (detailed under Materials and Methods), the whole-cell currents were conducted exclusively by hKv1.3 channels [25]. Representative current traces are shown in Fig. 3A. Macroscopic K^+ currents through hKv1.3 channels were recorded sequentially in the same cell, before (control traces) and after the addition of 10 nM sVmKTx to the external solution through perfusion. The Kv1.3 current almost completely disappeared by the 7th pulse (corresponding to 105 s) in the presence of 10 nM sVmKTx. Washing the perfusion chamber with toxin-free solution resulted in a full recovery from block (see Fig. 3C).

The kinetics of the development of the block of the whole-cell Kv1.3 current in T cells is shown in Fig. 3B for 3 nM sVmKTx and in Fig. 3C for 1 nM sVmKTx. The Kv1.3 current is progressively blocked by sVmKTx, which is reflected by decrease in the normalized peak currents as a function of time, the origin (t = 0) corresponds to the start of the perfusion with the toxin-containing extracellular solution. The comparison of Fig. 3B and C clearly indicates that equilibrium block

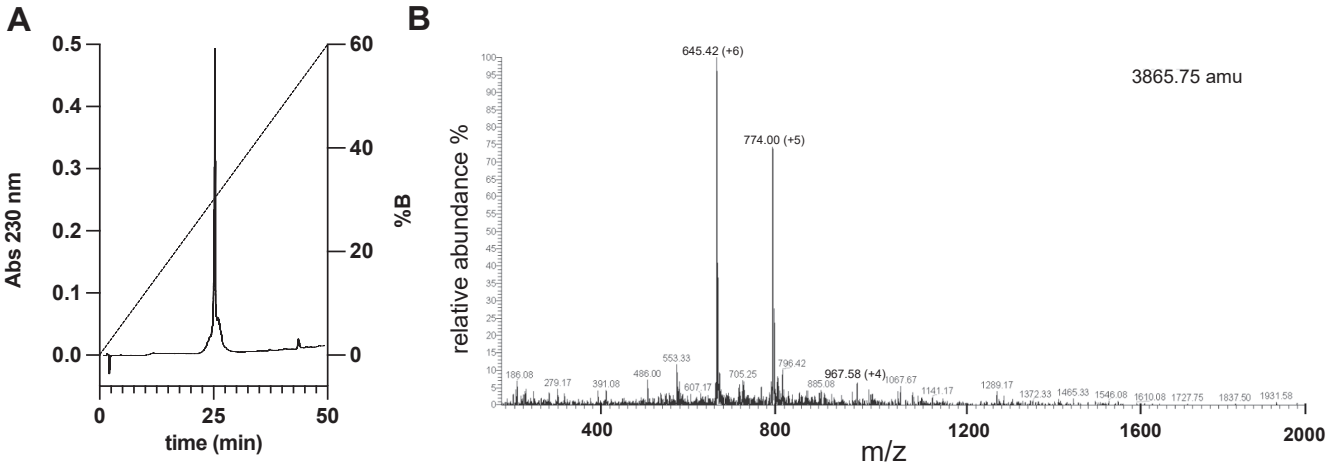

Fig. 2. Purification and validation of sVmKTx. (A) Purification of sVmKTx. A C18 analytical column (218TP54 Vydac) was used for the second separation as shown here, using a linear gradient from solvent A (0.12% TFA in water) to 60% solution B (0.1% TFA in acetonitrile) in 50 min. (B) Mass spectrometry analysis of purified peptide sVmKTx showing three main ions (645.42 of charge +6, 774.00 of charge +5 and 967.58 of charge +4) all corresponding to an unique peptide with 3865.75 atomic mass units (amu).

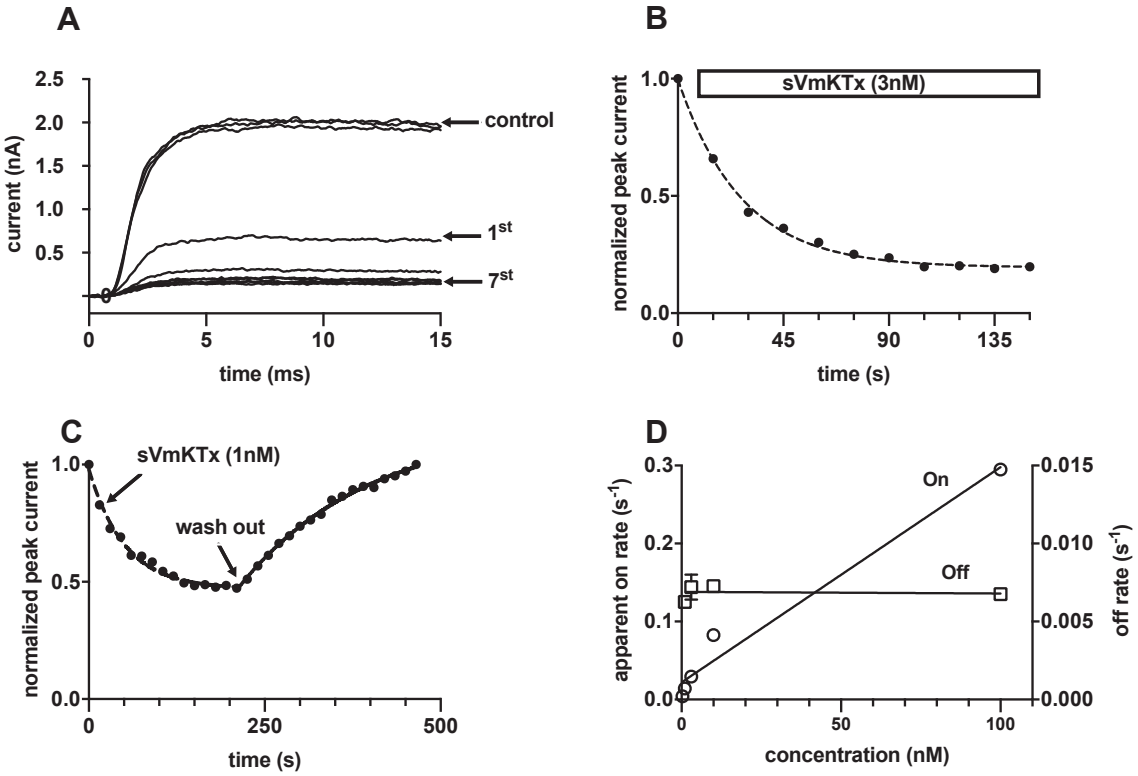

Fig. 3. Block of Kv1.3 channels by sVmKTx. A, whole-cell potassium currents through hKv1.3 channels evoked from a human T cell in response to depolarizing pulses to +50 mV from a holding potential of –120 mV every 15 s. Kv1.3 currents were almost completely blocked when the bath was perfused with 10 nM sVmKTx in the extracellular solution. Arrows indicate K^+ current in the absence of the toxin (control), and the 1st and 7th pulses in 10 nM sVmKTx. B, Kinetics of the block. Normalized peak currents are plotted as a function of time. The box indicates the application of the toxin-containing extracellular solution (3 nM sVmKTx). Dashed line indicates the fitting of a single-exponential decaying function to the data points resulting in τ_{in} = 51.2 s (see Materials and Methods). C, Peak currents were determined and normalized to the peak current in control solution, and values were plotted as a function of time. The arrows indicate the start of the perfusion with 1 nM sVmKTx and the wash-out using toxin-free extracellular solution (wash-out). Dashed line indicates the fitting of a single-exponential decaying function to the data points resulting in τ_{in} = 49.7 s. Perfusion with toxin free medium resulted in full recovery from block, with a time constant of τ_{out} = 169 s. Pulses were delivered every 15 s. D, effect of sVmKTx concentration on blocking kinetics. Apparent first order association (On, k_{on} × [sVmKTx], left ordinate, empty circles) and dissociation (Off, k_{off}, right ordinate, empty squares) rates were plotted as a function of the sVmKTx concentration. Data points were fitted with a linear function (solid lines r^2 = 0.99), error bars indicate SEM (n = 3).

develops faster for higher peptide concentration (150 s for 3 nM vs. 250 s for 1 nM). For both peptide concentrations, the kinetics of the block followed a single exponential time-course indicating a simple bimolecular interaction between the peptide and the channel.

Fig. 3C also shows, that the block of the Kv1.3 current is reversible. Upon equilibration of the block (~50% of the current is blocked at 1 nM sVmKTx) the extracellular solution was switched to a toxin-free extracellular solution (washout) resulting in a full recovery from block. Similar to the development of the block the wash-out phase followed a single exponential time course as well, the solid line superimposed on the data points indicates the best-fit single exponential function.

Fig. 3D shows the analysis of kinetic features of the development of current inhibition at various sVmKTx concentrations. The time constants for the development of the block (τ_{in}, association or wash-in time constant) were determined by fitting a single-exponential decay function to the normalized peak current–time relationships (Fig. 3B and C). The time constant for the recovery from block (τ_{out}, dissociation or wash-out time constant) was determined by fitting a single exponential rising function to the normalized peak currents-time relationship segment after the start of the wash-out (Fig. 3C). With the assumption of a bimolecular reaction between the toxin and the channel, the resulting wash-in time constant $\tau_{in} = 1/((k_{on} \times [sVmKTx] + k_{off})$ and the wash-out time constant is $\tau_{out} = (k_{off})^{-1}$, where k_{on} and k_{off} are the rate constants of toxin association to and dissociation from the channel, respectively, and [sVmKTx] is the peptide concentration. Plotting the apparent first-order rate constants for association (k_{on} × [sVmKTx]) and dissociation rate (k_{off}) values as a function of the sVmKTx concentrations showed that the apparent first-order association rate increases linearly with toxin concentration, whereas the dissociation rate remains constant: $k_{off} = 0.0069 \pm 0.00019\ s^{-1}$ [47]. The second order rate constant for association determined from the linear regression fit to the data points in Fig. 3D resulted in $k_{on} = 0.0085\ nM^{-1}\ s^{-1}$ (r^2 = 0.99).

To determine the concentration-dependence of current inhibition by sVmKTx, experiments shown in Fig. 3A–C were repeated at various sVmKTx concentrations ranging from 0.1 nM to 100 nM and remaining current fractions were determined upon reaching equilibrium block. The dose–response relationship was analyzed by fitting the Hill equation to the data points (Fig. 4), which yielded an equilibrium dissociation constant of 0.77 nM and a Hill coefficient of 1.1. The K_d obtained from equilibrium block is in good agreement with the dissociation constant calculated from the block kinetics, $K_d = k_{off}/k_{on} = 0.0069\ s^{-1}/0.0085\ nM^{-1}\ s^{-1} = 0.81$ nM. This confirms our assumption that the interaction between sVmKTx and the ion channel is bimolecular.

3.3. *sVmKTx is selective for Kv1.3 and does not inhibit a wide range of other channels*

Among the channels involved in the selectivity screening, the main targets were hKv1.1, hKv1.2 and hKCa3.1 since these channels were partially blocked by Vm24 at high, 10 nM concentration [25]. In addition to hKv1.1 (Fig. 5A), hKv1.2 (Fig. 5B) and hKCa3.1 (Fig. 5F), we also tested the effects of sVmKTx on the currents of the following five K^+

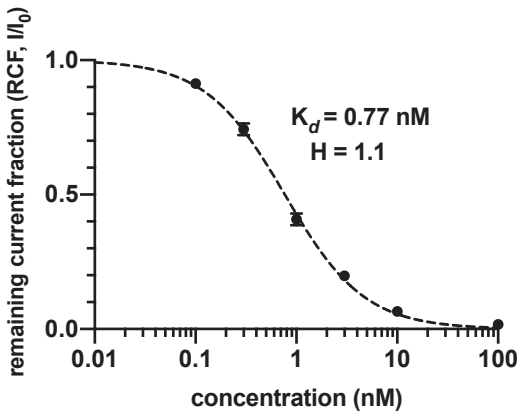

Fig. 4. Dose-response relationship for sVmKTx. The dose–response was obtained by plotting the remaining current fraction (RCF = I/I_0) as a function of toxin concentration (where I and I_0 are the peak currents measured in the presence and absence of toxin, respectively) and fitting the function RCF = $K_d^H/(K_d^H + [Tx]^H)$ to the data points (where [Tx] indicates the toxin concentration and K_d is the dissociation constant and H is the Hill coefficient). The superimposed dashed line is the Hill equation fitted to the data points (see Materials and Methods). The best fit yielded K_d of 0.77 nM, and H = 1.1. Error bars indicate SEM (n = 3–6).

channels and the human cardiac Na^+ channel: hKv1.4ΔN (fast inactivation-removed hKv1.4) (Fig. 5C), hKv1.5 (Fig. 5D), rKv2.1 (Fig. 5E), hKCa1.1 (Fig. 5G), hKv11.1 (Fig. 5H), and hNav1.5 (Fig. 5I). Of the tested channels, hKCa3.1, hKv1.1, and hKv1.2 were not blocked by sVmKTx at 100 nM, which is more than100-fold concentration than the K_d for Kv1.3, moreover, other channels studied were unaffected by 100 nM sVmKTx either (Fig. 6A).

Although Vm24 has more than 1500-fold selectivity over other channels, the peptide significantly inhibited the hKv1.1, hKv1.2 and hKCa3.1 currents at 10 nM concentration, which is more the 3300-fold concentration that the K_d for Kv1.3 (3 pM). Thus, we also tested sVmKTx at comparable concentrations, i.e., at 2.5 μM, which is more that 3200-fold concentration than the K_d for Kv1.3 (0.77 nM). sVmKTx in 2.5 μM concentration had no effect on hKv1.1 and KCa3.1 channels but it showed a partial (~25%) block of the hKv1.2 current (Fig. 6B and C), the RCF value was 0.74 ± 0.007 (n = 3). The estimated K_d value for hKv1.2 from a single concentration, based on a bimolecular interaction, yielded 7.1 μM. The material available was not sufficient to construct a full concentration–response study at this very high peptide concentration range.

3.4. Comparison of Vm24 and sVmKTx structure

The sequence of sVmKTx differs from Vm24 only in one amino acid residue (K32E), therefore the NMR structure of the latter (PDB ID: 2K9O) [26] can serve as an initial estimate for the 3D structure of the mutated peptide (see Materials and Methods for details). Replica exchange solute tempering molecular dynamics was used to create a representative sample of Vm24 and sVmKTx conformations at 300 K. Fig. 7A presents the root-mean-square fluctuations (RMSF) of heavy atoms of the amino acid residues of both toxins. The fluctuations are considerably smaller owing to the K32E mutation in the sVmKTx toxin. The main reason of this change is the formation of new H-bonds between the E32 and K30, A1 and R17 residues (Fig. 7B and C) appearing in 30%, 43% and 26% of the trajectory, respectively. These H-bonds cannot be formed in the case of Vm24 with a lysine at position 32 in its sequence. The RMSF values for the channel-bound toxins (see below for details on docking) are also displayed in Fig. 7A (dotted lines) along with those of the free toxins in solution (solid lines). The fluctuations decrease for most of the residues of Vm24 and sVmKTx after binding to hKv1.3 as compared to the free toxins. However, the N-terminal region of Vm24 remained more flexible than that of sVmKTx even after binding to the channel.

3.5. Interaction patterns of Vm24 and sVmKTx toxins with the hKv1.3 ion channel

Homology model of the human Kv1.3 channel (UniProt ID: P22001) was created for the inner region of the channel, (amino acid residues 383–491). X-ray structure of ChTx bound Kv1.2-2.1 chimera ion channel (*Rattus Norvegicus*, PDB ID: 4JTA) [34] was used as a template. The ToxDock protocol in the Rosetta package [35] was used to find the best docking poses of Vm24 and sVmKTx to the homology model of the human Kv1.3 channel. Five structures with the highest surface interaction were selected from the 25 highest ranked docking poses for further molecular dynamics calculations. Five MD simulations of 100 ns duration (Schrödinger Release 2019-4, Schrödinger, LLC, New York, NY) were used to generate a statistically acceptable sample of conformations for the characterization of the interactions of Vm24 and sVmKTx toxins with Kv1.3. The RMSF values of the non-H atoms of the residues of both toxins were calculated similarly to their free states. Finally, a single trajectory MM-GBSA binding free energy calculation [42] was carried out on the collected samples to elucidate the differences of the interaction patterns of the toxins, using partitioned, per-residue contributions of the total binding free energy [45] (see Materials and Methods for details).

The MM-GBSA method provided binding free energy estimates of −104.1 ± 4.7 kcal/mol and −89.9 ± 5.3 kcal/mol for the toxins Vm24 and sVmKTx, respectively. Per-residue contributions to the MM-GBSA binding free energy were calculated for residues within 8 Å of the toxins. The differences of the dominant contributions were calculated by subtracting the values belonging to the Vm24 complex from those of sVmKTx complex ($dG_{sVmKTx} - dG_{Vm24}$) and presented in Fig. 8A. These differences elucidate the changes in the interaction pattern caused by the K32E amino acid substitution. Binding free energy contributions from residues M27, N28, K32, Y34 became less negative resulting in positive differences. This shows weakened interactions. Binding free energy contributions from residues C26 and R29 became more negative indicating stronger interactions. Overall, weakening dominates, therefore K32E mutation results in smaller binding affinity in the case of toxin sVmKTx. Per-residue contributions to MM/GBSA binding free energy were also calculated for the ion channel residues within 8 Å of the toxins. Differences of these contributions of sVmKTx-Kv1.3 and Vm24-Kv1.3 complexes were also calculated, and dominant contributions are shown in Fig. 8B. The largest positive differences in per residue contributions belong to H451 residues in two adjacent chains A and D, representing weaker interactions (the numbering of channel amino acid residues is according to Fig. 8C). On the other hand, the dominant negative values correspond to H451 and D449 of chain B.

3.6. sVmKTx inhibits CD40L expression in $CD4^+$ T cells

CD40L expression reports on the efficacy of early, Ca^{2+}-dependent activation steps in human $CD4^+$ T cells and has been used as a readout to assess Kv1.3-dependence of T cell activation [48,49]. We induced CD40L expression by direct stimulation of the T cell receptor pathway with αCD3/αCD28 DynaBeads in human $CD4^+$ T cells and determined the fraction of cells expressing CD40L using flow cytometry. The time course of the generation of CD40L expressing cells was determined by starting a 24 h assay following αCD3/αCD28 stimulation and samples were obtained at different time points for CD40L staining. Fig. 9A shows that the αCD3/αCD28 stimulation-induced increase in the fraction of CD40L expressing cells saturates by 24 h, by this time point 74.9 ± 0.5% (SEM, n = 7) of the cells showed CD40L expression. In the next step, we determine if sVmKTx reduced the fraction of T cells expressing CD40L upon αCD3/αCD28 stimulation. Based on the data in Fig. 9A, we set the

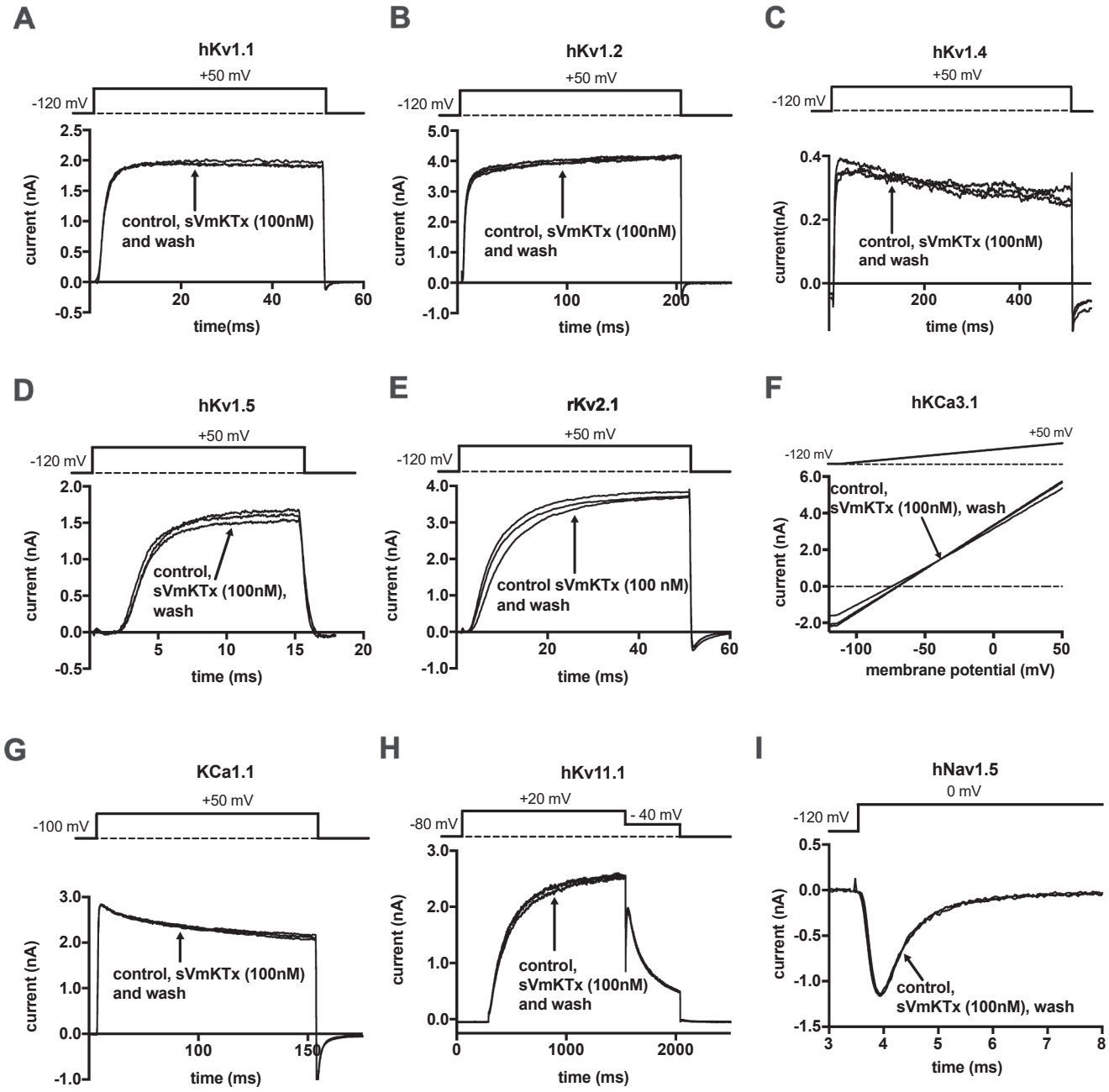

Fig. 5. 100 nM sVmKTx has no effect on several ion channels. Current traces recorded before the application of the toxin (control), after 10 sweeps in 100 nM sVmKTx, and after perfusing the recording chamber with control solution (wash out of the toxin). Data are shown for the following channels: hKv1.1 (A), hKv1.2 (B), fast inactivation-removed hKv1.4 (Kv1.4ΔN) (C), hKv1.5 (D), rKv2.1 (E), hKCa3.1 (F), hKCa1.1 (hBK) (G), hKv11.1 (hERG) (H) and hNav1.5 (I) (for details on the expression systems, solutions, and voltage protocols, see Materials and Methods).

duration of the αCD3/αCD28 exposure to 5 h in the subsequent experiments, which leads to a measurable increase in CD40L expressing cells, however, the IL-2 induced auto activation of the cells can be avoided (Fig. 9A) [50]. $CD4^+$ cells were pre-incubated for 5 min with sVmKTx (100 nM) and cells were then activated for 5 h with αCD3/αCD28 DynaBead in the continuous presence of sVmKTx. The flow cytometric histograms in Fig. 9B show that 100 nM sVmKTx has substantially reduced the fraction of CD40L expressing the T cells (green trace) as compared to the control cells stimulated identically in the absence of sVmKTx (red trace). Fig. 9C shows that the fraction CD40L expressing cells in the presence of sVmKTx, normalized to that of stimulated cells in the absence of the toxin, is reduced to ~50% (n = 3). Cells not exposed to αCD3/αCD28 beads showed practically no CD40L expression.

4. Discussion

We characterized the *in vitro* pharmacological properties and biological effect of the sVmKTx peptide synthetized based on the transcriptome analysis of the venom gland of the Mexican scorpion *V. mexicanus smithi* [17]. We showed that sVmKTx is a high-affinity inhibitor of Kv1.3 channels with a K_d of 770 ± 21 pM (Fig. 4). The Kv1.3 selectivity of sVmKTx is at least 6-fold greater than that of Vm24 over the battery of ion channels tested in this study (Figs. 5 and 6). Based on molecular dynamics simulations, we report decreased flexibility of sVmKTx over Vm24 both in solution and bound to Kv1.3. MM-GBSA binding free energy calculations predicted unfavorable interactions between sVmKTx and H451 in neighboring subunits of the channel, which

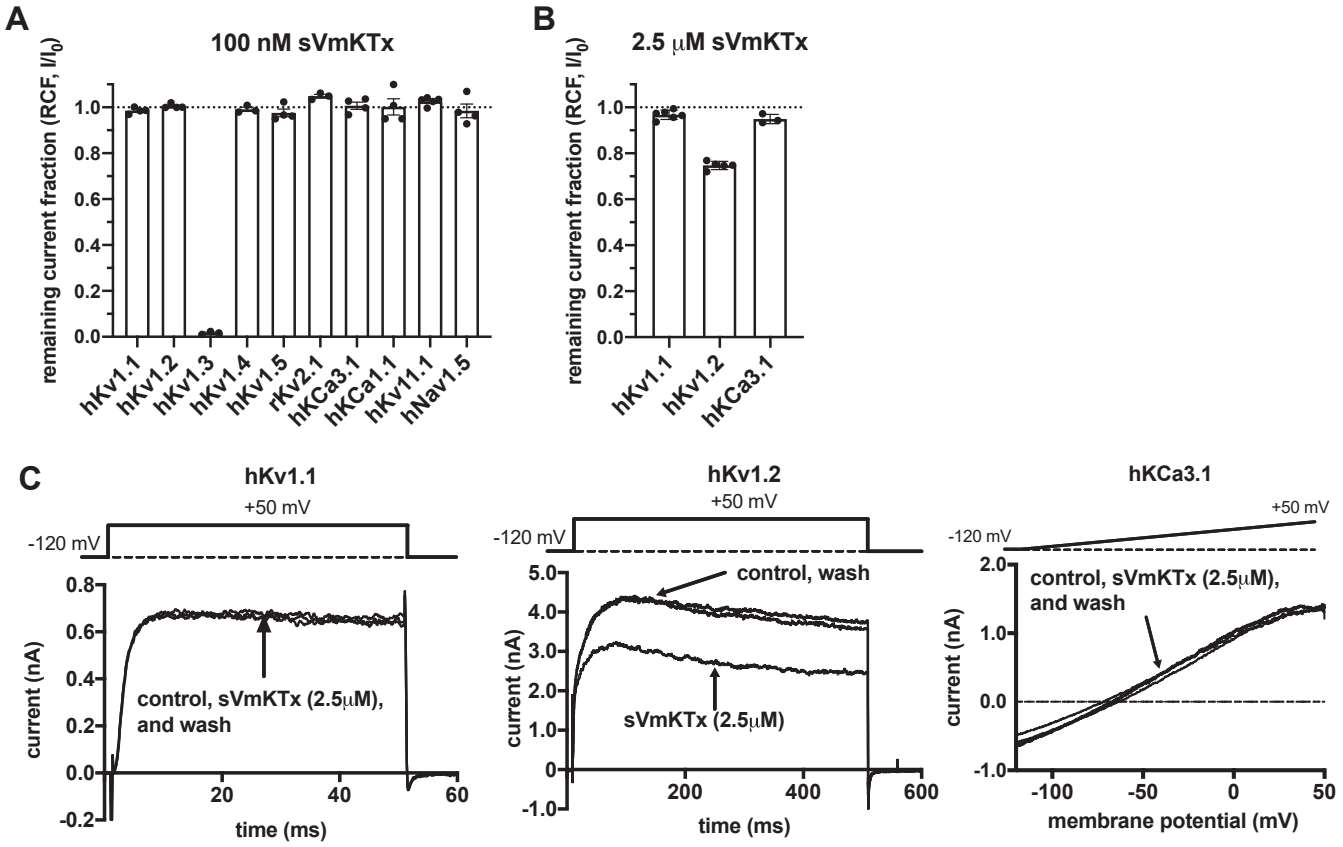

Fig. 6. Selectivity of sVmKTx for Kv1.3 channels. A, remaining current fractions for the indicated channels. RCF values were calculated at equilibrium block (for Kv1.3) or following 10 repeated depolarizations in the presence of sVmKTx applied at 100 nM concentration. Data are presented as mean ± SEM ($n \geq 3$, independent data points are indicated by filled circles). B, remaining current fractions for hKv1.1, hKv1.2 and hKCa3.1 at 2.5 μM sVmKTx concentration. Data are at equilibrium block (for hKv1.2) or after 10 repeated depolarizations in the presence of 2.5 μM sVmKTx (for hKv1.1 and hKCa3.1). Data are represented as in panel A. C, effects of 2.5 μM sVmKTx on hKv1.1, hKv1.2, and hKCa3.1 currents. Current traces recorded before the application of the toxin (control), after the equilibration of block (or 10 pulses in the presence of the toxin if block was not apparent) at 2.5 μM sVmKTx, and after perfusing with control solution (wash out of the toxin) are indicated (for details on the expression systems, solutions, and voltage protocols, see Materials and Methods).

may explain the lower affinity of sVmKTx for Kv1.3 compared with Vm24. Nevertheless, sVmKTx in nanomolar concentrations inhibited the activation of human $CD4^+$ T lymphocytes *in vitro*.

sVmKTx is a 36-amino acid peptide toxin stabilized by four disulfide bridges that contains a highly conserved pair of residues (K25 and Y34) that may constitute the functional dyad characteristic of many K^+ channel blocker scorpion toxins [51]. sVmKTx differs from Vm24, a well characterized peptide inhibitor isolated from *V. mexicanus smithi,* by only one amino acid residue at position 32. At physiological pH values Vm24 contains a positively charged lysine, whereas sVmKTx contains a negatively charged glutamate at that position (Fig. 1). Based on the high sequence similarities, we hypothesized that sVmKTx inhibits Kv1.3 channel in similar manner as Vm24 [25]. That is, the peptide binds to the external vestibule of the channel in the pore domain and consequently physically occludes the ion permeation pathway, as it has been shown experimentally for ChTx [47]. Based on the sVmKTx concentration dependence of the *on* and *off* rates (Fig. 3D) sVmKTx interacts with Kv1.3 in a simple bimolecular manner, which is consistent with the interaction of pore blocker toxins [47]. Moreover, the dissociation constant calculated by the k_{off}/k_{on} ratio ($K_d = 0.81$ nM) is very close to the one determined by fitting the Hill equation with Hill coefficient of 1.1 to the concentration dependence of current inhibition ($K_d = 0.77$ nM).

As compared with Vm24, one of the key features of sVmKTx block of Kv1.3 is the full reversibility within 300 s after switching to toxin-free solution (Fig. 3C). We hypothesized that the presence of a negatively charged E32 in sVmKTx may create an unfavorable interaction with Kv1.3 that finally results in the increased off rate compared to Vm24 that contains a positively charged lysine at the same position. The analysis of the rate constants showed that both k_{on} and k_{off} are altered: the k_{on} decreased ~10-fold ($k_{on} \sim 0.0955$ $nM^{-1}s^{-1}$ for Vm24 [25] vs $k_{on} = 0.0085$ $nM^{-1}s^{-1}$ for sVmKTx), which was accompanied by a ~25-fold increase in the k_{off} of sVmKTx to account for the overall ~250-fold decrease in the Kv1.3 affinity of this peptide for Kv1.3 as compared to Vm24. Consistent with this, the largest contribution to the less favorable free energy of binding of sVmKTx, as compared to Vm24, can be attributed to the amino acid residue at position 32 (Fig. 8A). The K32E substitution weakened the binding of sVmKTx to H451 of Kv1.3 in chains A and D of the tetramer and simultaneously strengthened the binding of residue R29 of the toxin to H451 in chain B. This partial compensation of the binding free energy changes can be the origin of the still high (~sub-nanomolar) affinity of sVmKTx toxin for Kv1.3. The R34Q substitution at the equivalent position in ChTx resulted in a ~300-fold decreased affinity for Shaker (F425G) with ~3-fold decrease in the association rate and ~100-fold increase in the k_{off} [52]. Charge reversal mutation of ChTx at this position (either R34E or R34D) resulted in a complete loss of affinity for Shaker (F425G). This indicates that in addition to the essential diad residues, a positively charged residue at position 34 in ChTx and at position 32 in Vm24 is required for high affinity binding of the toxins to their respective target channel.

The most potent peptide blockers of Kv1.3 inhibit the K^+ current at low picomolar concentrations. These peptides include the sea anemone toxin ShK (Kd ~ 11 pM, [53,54]) and the toxins isolated from scorpion venoms such as margatoxin (MgTx, $K_d = 50$ pM) [55,56], OSK1 ($K_d = 17$ pM, [57]) and *Heterometrus spinifer* Toxin 1 (HsTx1, $K_d = 12$ pM) [58].

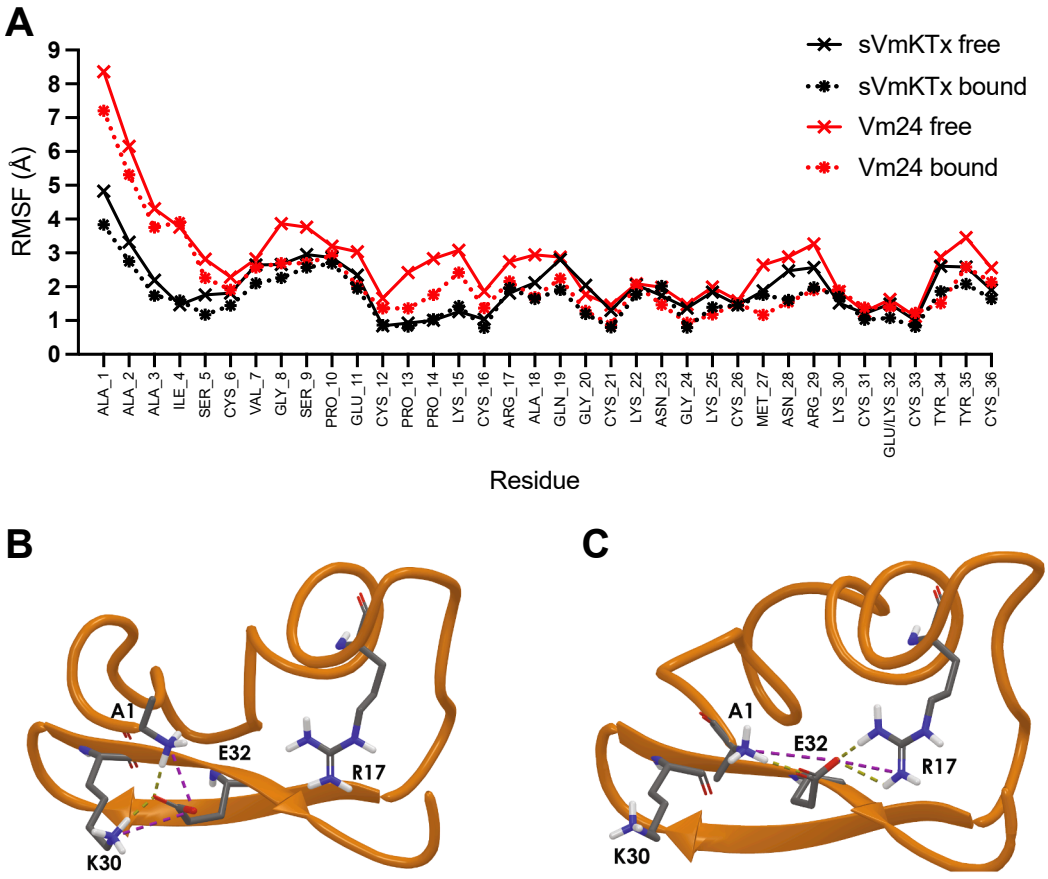

Fig. 7. (A) Root-mean-square fluctuations of the non-H atoms of amino acid residues of sVmKTx (black) and Vm24 (red) toxins obtained for their free (solid lines, ×) and hKv1.3-bound state (dotted lines, *). (B, C) Representative H-bonds formed by E32 in sVmKTx toxin with residues A1, R17 and R30. (For interpretation of the references to colour in this figure legend, the reader is referred to the web version of this article.)

The selectivity of these peptides for Kv1.3 is limited, which is reflected in their ability to inhibit Kv1.1 and/or Kv1.2 with similar potency (e.g., Kv1.1 or Kv1.2 [28,56,59,60]. A clear contrast to these is Vm24 (α-kTx23.1) that inhibits Kv1.3 with high affinity (K_d ~ 3 pM) and displays a ~1500-fold selectivity for Kv1.3 over several ion channels including Kv1.1 and Kv1.2 [25], although Vm24 is the member of a the α-KTx family, admits unique three-dimensional structural features such as an extra β-strand and a loosely defined α-helix segment [26]. The functional dyad located at the C-terminal β-hairpin is conserved for most of the pore blocking α-KTx peptides but the selectivity of Vm24 against Kv1.3 may rely on the unique N-terminal segment (residues A1-E11) making extensive contacts with the ion channel [26]. Furthermore, the non-conserved E11 of Vm24 binds to the H451 residue of Kv1.3, a position that has been identified as critical determining the affinity of several toxins for Kv1 channels [26,61]. We propose that the single amino acid substitution at position 32 of Vm24 that produces sVmKTx does not induce gross conformational changes in the peptide and the nature of its interaction with the Kv1.3, similar to many substitutions in other toxins (OSK1 analogues [57]), AnTx analogues [62]. The results of our homology modeling-based binding free energy calculation and docking are consistent with the maintained overall structure of sVmKTx and its interaction with Kv1.3.

Recent reviews analyzed in detail the strategies by which the selectivity of toxins can be increased for Kv1.3 [63,64]. These include *chemical modification* (e.g. in case of ShK-Dap^{22}, the substitution by an unnatural amino acid, [65]), *truncation* (e.g. in case of [Δ36–38]-OSK1-E16K/K20D peptide, combined with chemical modification [66]), *reorientation of the binding interface* of the toxins by modifying acidic residues (e-g- in case of BmKTX-19 and BmKTX-196, [67]) and *reducing the conformational flexibility of the toxin*, as in case on [N17A/F32T]-AnTx [62]. In this latter case, the natural peptide (AnTx) inhibited Kv1.3 and Kv1.2 with almost equal potency, whereas the double substituted peptide was ~16,000-fold more selective for Kv1.3 over Kv1.2. Structural analysis combined with molecular dynamics simulations indicated that [N17A/F32T]-AnTx possessed a more rigid structure than the flexible wild-type AnTx, with a large fraction of the structural uncertainty in AnTx located in the loop between the N-terminal and the first helical element (residues 5–9). Our molecular dynamics simulations are consistent with these findings, i.e., the introduction of a glutamate instead of lysine at position 32 led to a decreased structural fluctuation of the N-terminal segment of sVmKTx compared to that of Vm24. This difference was preserved even after their binding to hKv1.3. Thus, the reduced conformational flexibility of sVmKTx may explain the increased selectivity of the peptide for Kv1.3 as compared to Vm24, like in [N17A/F32T]-AnTx vs. AnTx. The selectivity is improved even if the unfavorable interaction between E32 and H451 weakens the binding of the toxin to Kv1.3.

sVmKTx displayed a unique selectivity profile; it did not inhibit hKv1.1, hKv1.2, hKv1.4, hKv1.5, rKv2.1 hKCa3.1, hKCa1.1, hKv11.1 and hNav1.5 at 100-fold higher concentration than the K_d for Kv1.3, which is a commonly accepted criterion for a selective blocker [68]. The only ion channel inhibited by sVmKTx was Kv1.2 at very high peptide concentration (2.5 μM concentration, that is 3200-fold the K_d for Kv1.3), the single point estimate of the Kd was (~7.1 μM) that makes sVmKTx ~9,000-fold selective over Kv1.2. A similar experiment using Vm24 showed ~1500-fold selectivity for Kv1.3 over Kv1.2, thus, sVmKTx has ~6-fold better Kv1.3 selectivity than Vm24. More importantly, to target selectively autoreactive T_{EM} cells of Kv1.3^{high} channel phenotype the

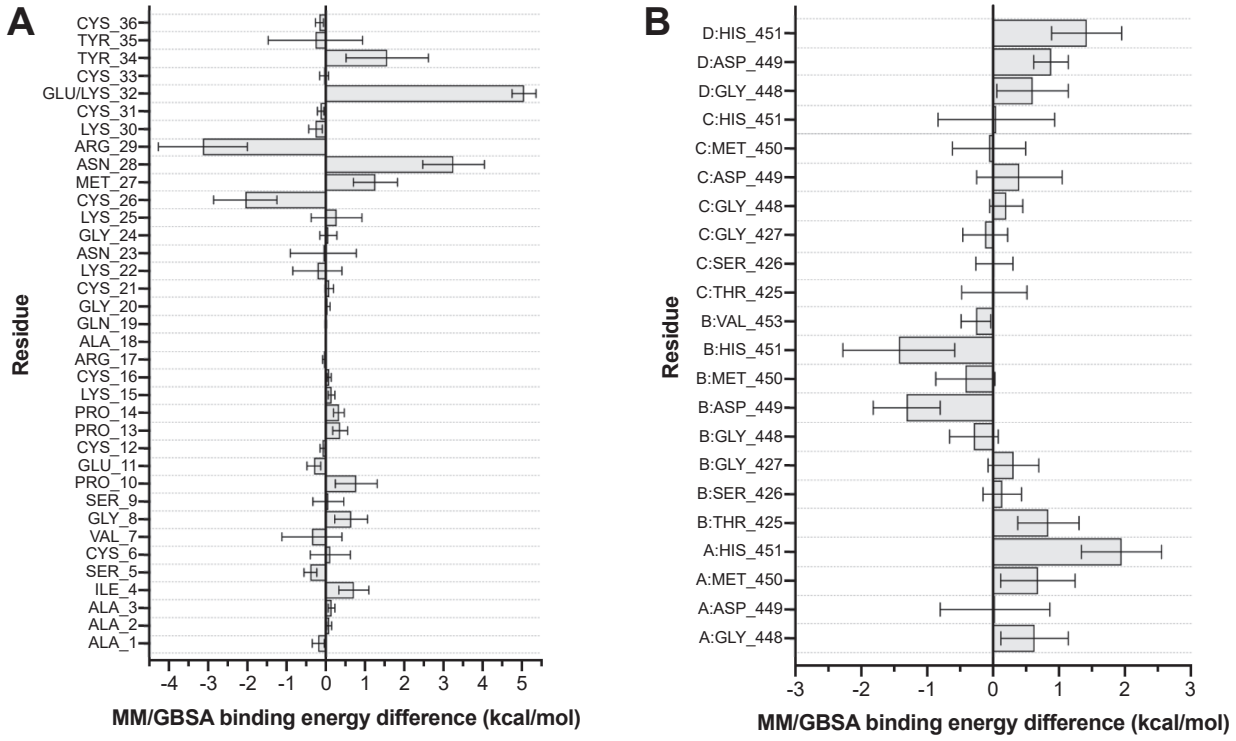

C

hKv1.3	383	GLQILGQTLKASMRELGLLIFFLFIGVILFSSAVYFAEADDPTSGFSSIPDAFWW	437	100%
4JTA_A	309	GLQILGQTLKASMRELGLLIFFLFIGVILFSSAVYFAEADERDSQFPSIPDAFWW	363	93%
hKv1.3	438	AVVTMTTVGYGDM**H**PVTIGGKIVGSLCAIAGVLTIALPVPVIVSNFNYFYHRET	491	100%
4JTA_A	364	AVVSMTTVGYGDM**V**PTTIGGKIVGSLCAIAGVLTIALPVPVIVSNFNYFYHRET	417	93%

Fig. 8. Differences of per-residue to the MM-GBSA binding free energy of the toxins in the sVmKTx-hKv1.3 and Vm24-hKv1.3 complexes for the toxin residues (A) and the pore region of hKv1.3 (B). Binding energy differences were calculated as $dG_{sVmKTx} - dG_{Vm24}$ for each residue of the peptide (A) and the ion channel (B). Capital letters preceding the positions in panel B indicate chain (A-D) of the tetrameric channel. Error bars show SEM calculated with the bootstrap method (see main text). (C) Sequence alignment of human voltage-gated potassium channel subunit Kv1.3 and the Kv1.2–2.1 chimera ion channel (*Rattus Norvegicus*, PDB ID: 4JTA) [34]. The sequence identity is on the right (%), residue H451 of Kv1.3 and the corresponding V377 of Kv1.2–2.1 chimera are in bold and underlined.

peptide must be selective for Kv1.3 over KCa3.1 channels expressed in non-T_{EM} immune and other cells [18,63]. sVmKTx is far superior to Vm24 in this respect as sVmKTx does not inhibit KCa3.1 at very high, 2.5 μM concentration whereas the inhibition of KCa3.1 was ~50% at the equivalent concentration of Vm24. The order of the blocking potency of Vm24 for various ion channels was hKv1.3 ≫ hKv1.2 > hKCa3.1 > mKv1.1 ≫ hKv1.4 ≈ hKv1.5 ≈ rKv2.1≈ hKv11.1 ≈ hKCa1.1 ≈ hKCa2.3 ≈ hNav1.5 [25], whereas for sVmKTx it was hKv1.3 ≫ hKv1.2 ≫ hKCa3.1 ≈ hKv1.1 ≈ hKv1.4 ≈ hKv1.5 ≈ rKv2.1 ≈ hKCa1.1 ≈ hKv11.1 ≈ hNav1.5 (Figs. 5 and 6). The Kv1.3 selectivity of sVmKTx is outstanding, the closest in the rank are Vm24 (~1500-fold, [25]) and R14A-HsTx1 (2000-fold [60]) followed by other Kv1.3 selective peptides ([Lys16,Asp20]-OSK1 [57], [Arg11,Thr28,His33]-BmKTx [69], and ShK(L192) [70] for which toxin selectivity ranged between 9- and 340-fold).

The potency of sVmKTx as a potential immunosuppressor peptide was demonstrated in a functional assay where CD40 ligand expression was measured following activation of the T cells. CD40 ligand is an early, Ca^{2+}- and NFAT-dependent activation marker of the T cells [71]. Since Kv1.3 controls Ca^{2+} signaling, thus the expression level of the CD40L, particularly in the effector memory T cells, inhibition of these channels leads to a decreased expression level of this early activation marker [72]. We obtained the time-course of the expression of the early activation marker CD40L in this experiment (Fig. 9A) to avoid the IL-2 induced auto activation of the cells, which may mask the effect of the ion channel blockers [50]. sVmKTx significantly inhibited the TCR-mediated CD40L upregulation, which is consistent with the literature and confirms the role of the Kv1.3 ion channels in the TCR-mediated T cell activation via promotion the Ca^{2+} influx [24,73]. Previous studies also confirmed that the inhibition of T cell activation results in the prevention and the treatment of experimental autoimmune disease in animals as Kv1.3 inhibitors persistently suppress the proliferation of T_{EM} cells [19–21,74]. However, the sVmKTx concentration that completely blocks Kv1.3 (~100-fold the K_d) causes only a partially inhibition in the CD40L expression only. The reason for this partial inhibition might be that the $CD4^+$ lymphocytes we used in the experiments contain other T cell subpopulations like naïve and central memory T cells, in which the dominant KCa3.1 ion channels provide the electrical driving force for calcium entry resulting in T cell activation [75].

In conclusion, sVmKTx is novel peptide produced recombinantly based on the transcriptome analysis of the scorpion *V. mexicanus*. sVmKTx displays exceptional Kv1.3 selectivity, which may be a useful tool to modulate autoimmune diseases and may serve as template for drug development targeting these diseases. The increase in its selectivity

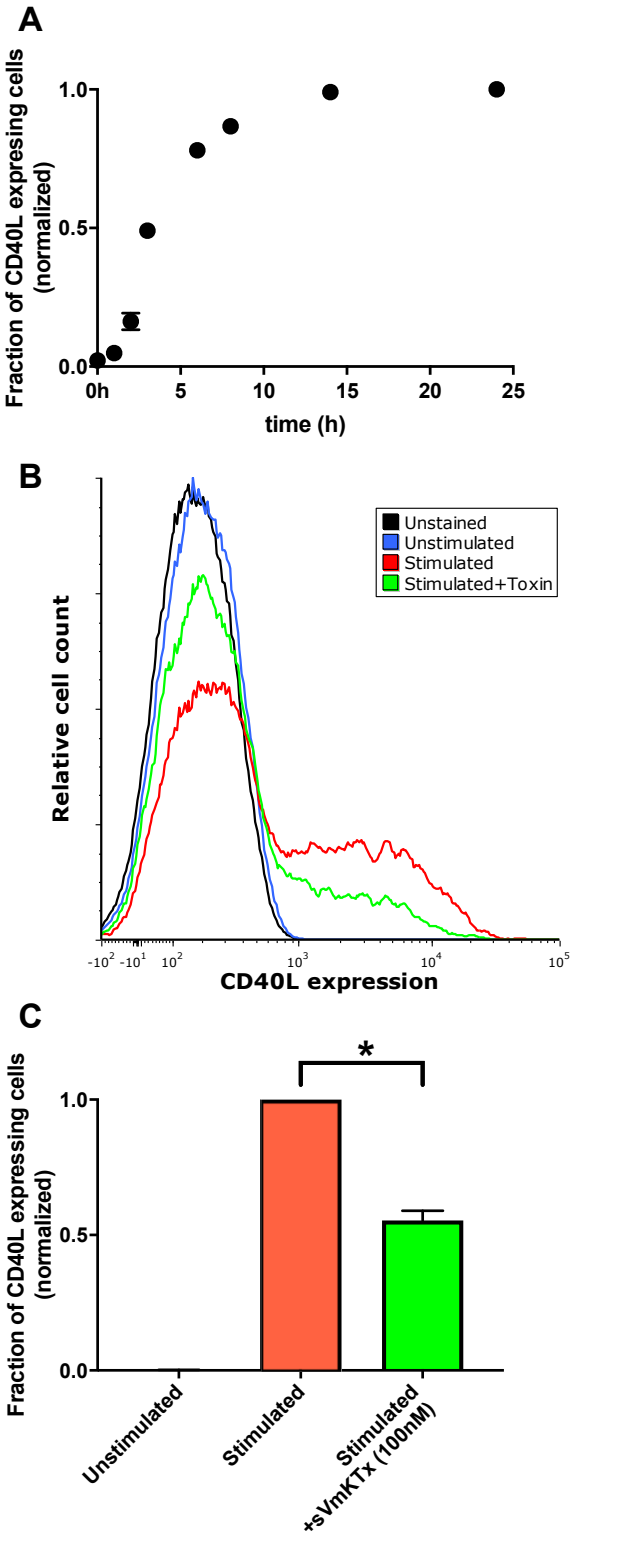

(caption on next column)

Fig. 9. sVmKTx reduces the fraction of CD40L expressing CD4$^+$ T cells following stimulation. (A) The fraction of CD40L expressing cells upon αCD3/αCD28 DynaBead stimulation as a function of time. Cells were incubated for a maximum of 24 h in the presence of the DynaBeads, and the fraction of CD40L expressing cells was determined at the indicated time points using flow cytometry. After FSC-SSC gating, unstained controls were used to determine the gating strategy. The fraction of CD40L expressing cells was determined from the histograms and fractions obtained at different time points were normalized to the highest value at 24 h and plotted as a function of time (n = 3). (B) Representative flow cytometric histograms of CD40L expression in unstimulated CD4$^+$ T cells (blue), stimulated CD4$^+$ T cells (red), sVmKTx (100 nM)-treated stimulated CD4$^+$ T cells (light green) and unstained/unstimulated control (black). T cells were stimulated as in (A) and the data were collected 5 h after the activation with beads. The histograms were adjusted to identical areas under the curves, thus, the ordinate indicates relative cell count. (C) The fraction of CD40L expressing cells in the presence and absence of sVmKTx. Cells were stimulated and the fraction of T cells expressing CD40L were determined as in (B). Fraction of CD40L expressing cells in the presence of 100 nM sVmKTx were normalized to the sample obtained in the absence of sVmKTx. The unstimulated sample was not activated with the beads. Samples were run in triplicates; data were averaged for n = 3 independent experiments (mean ± SEM). Significance of pairwise comparisons between groups is indicated with asterisk. * = statistically significant difference (P = 0.018). (For interpretation of the references to colour in this figure legend, the reader is referred to the web version of this article.)

as compared to Vm24 was accompanied by a lower Kv1.3 affinity that can be attributed to the unfavorable interaction of E32 of the toxin and H451 of the channel. Nevertheless, sVmKTx still has sub-nanomolar affinity for Kv1.3, which makes it an attractive peptide for therapeutic use.

CRediT authorship contribution statement

Agota Csoti: Investigation, Writing – original draft, Visualization. **Rosby del Carmen Nájera Meza:** Investigation. **Ferenc Bogár:** Formal analysis. **Gabor Tajti:** Investigation. **Tibor G. Szanto:** Investigation, Methodology, Writing – review & editing. **Zoltan Varga:** Conceptualization, Formal analysis. **Georgina B. Gurrola:** Investigation. **Gábor K. Tóth:** Conceptualization, Formal analysis, Funding acquisition. **Lourival D. Possani:** . **Gyorgy Panyi:** Conceptualization, Writing – review & editing, Funding acquisition, Supervision.

Declaration of Competing Interest

The authors declare that they have no known competing financial interests or personal relationships that could have appeared to influence the work reported in this paper.

Acknowledgements

The authors would like to thank the technical assistance of Ms. Cecilia Nagy and Ms. Adrienn Bagosi. This work was supported by the following grants: National Research Development and Innovation Office, Hungary, grants OTKA 143071 and K119417 (G.P.) and OTKA K132906 (Z.V.); Ministry of Human Capacities, Hungary, grant EFOP-3.6.2-16-2017-00006 (G. Panyi, G. K. Tóth); and Ministry of Finance, Hungary, grant GINOP-2.3.2-15-2016-00044 (G. Panyi), Ministry of Human Capacities, Hungary grant, TKP-2020 (G.T), and grant PRONACE303045 from National Conseil of Science and Technology of Mexico (L.D.P.). We acknowledge KIFÜ for awarding us access to computational resources based in Debrecen, Hungary.

Author contributions

A.C.: electrophysiology assays, writing of the first draft, graphs.
RCNM: synthetic production of the peptide.
F.B.: binding energy and molecular dynamics simulation, writing.
GT: flow cytometry.
T.G.Sz: electrophysiology analysis, writing, statistical analysis.
Z.V.: conceptualizing the experiment, data analysis.
G.B.G: chemical synthesis and analysis of the peptide.
G.K.T: conceptualizing binding energy and molecular dynamics simulations.
L.D.P: conceptualizing the experiments, writing, and editing the manuscript, acquired funding.
G.P.: conceptualizing the experiments, writing, and editing the manuscript, acquired funding

References

[1] J.-P. Chippaux, M. Goyffon, Epidemiology of scorpionism: a global appraisal, Acta Trop. 107 (2) (2008) 71–79.
[2] R.C. Rodríguez de la Vega, E.F. Schwartz, L.D. Possani, E.F. Schwartz, L.D. Possani, Mining on scorpion venom biodiversity, Toxicon 56 (7) (2010) 1155–1161.
[3] Z. Fajloun, R. Kharrat, L. Chen, C. Lecomte, E. Di Luccio, D. Bichet, M. El Ayeb, H. Rochat, P.D. Allen, I.N. Pessah, M. De Waard, J.M. Sabatier, Chemical synthesis and characterization of maurocalcine, a scorpion toxin that activates Ca(2+) release channel/ryanodine receptors, FEBS Lett. 469 (2-3) (2000) 179–185.
[4] J.A. DeBin, J.E. Maggio, G.R. Strichartz, Purification and characterization of chlorotoxin, a chloride channel ligand from the venom of the scorpion, Am. J. Physiol. 264 (2) (1993) C361–C369.
[5] R.S. Norton, K.G. Chandy, Venom-derived peptide inhibitors of voltage-gated potassium channels, Neuropharmacology 127 (2017) 124–138.
[6] F. Bosmans, K.J. Swartz, Targeting voltage sensors in sodium channels with spider toxins, Trends Pharmacol. Sci. 31 (4) (2010) 175–182.
[7] C. Miller, E. Moczydlowski, R. Latorre, M. Phillips, Charybdotoxin, a protein inhibitor of single Ca^{2+}-activated K^{+} channels from mammalian skeletal muscle, Nature 313 (6000) (1985) 316–318.
[8] D.M. Housley, G.D. Housley, M.J. Liddell, E.A. Jennings, Scorpion toxin peptide action at the ion channel subunit level, Neuropharmacology 127 (2017) 46–78.
[9] V. Quintero-Hernández, J.M. Jiménez-Vargas, G.B. Gurrola, H.H. Valdivia, L. D. Possani, Scorpion venom components that affect ion-channels function, Toxicon 76 (2013) 328–342.
[10] L.D. Possani, B. Becerril, M. Delepierre, J. Tytgat, Scorpion toxins specific for Na+-channels, Eur. J. Biochem. 264 (2) (1999) 287–300.
[11] J. Tytgat, K.G. Chandy, M.L. Garcia, G.A. Gutman, M.F. Martin-Eauclaire, J.J. van der Walt, et al., A unified nomenclature for short-chain peptides isolated from scorpion venoms: alpha-KTx molecular subfamilies, Trends Pharmacol. Sci. 20 (11) (1999) 444–447.
[12] L.A.F. Ferreira, E.W. Alves, O.B. Henriques, Peptide T, a novel bradykinin potentiator isolated from Tityus serrulatus scorpion venom, Toxicon 31 (8) (1993) 941–947.
[13] A. Torres-Larios, G.B. Gurrola, F.Z. Zamudio, L.D. Possani, Hadrurin, a new antimicrobial peptide from the venom of the scorpion Hadrurus aztecus, Eur. J. Biochem. 267 (16) (2000) 5023–5031.
[14] É.R. Alvarenga, T.M. Mendes, B.F. Magalhães, F.F. Siqueira, A.E. Dantas, T. M. Barroca, et al., Transcriptome analysis of the Tityus serrulatus scorpion venom gland, Open J. Genet. 2 (2012).
[15] Y. Ma, R. Zhao, Y. He, S. Li, J. Liu, Y. Wu, Z. Cao, W. Li, Transcriptome analysis of the venom gland of the scorpion Scorpiops jendeki: implication for the evolution of the scorpion venom arsenal, BMC Genomics 10 (1) (2009), https://doi.org/10.1186/1471-2164-10-290.
[16] E.F. Schwartz, E. Diego-Garcia, R.C. Rodríguez de la Vega, L.D. Possani, Transcriptome analysis of the venom gland of the Mexican scorpion Hadrurus gertschi (Arachnida: Scorpiones), BMC Genomics 8 (1) (2007), https://doi.org/10.1186/1471-2164-8-119.
[17] V. Quintero-Hernandez, S. Ramirez-Carreto, M.T. Romero-Gutierrez, L.L. Valdez-Velazquez, B. Becerril, L.D. Possani, et al., Transcriptome analysis of scorpion species belonging to the Vaejovis genus, PLoS One 10 (2) (2015) e0117188.
[18] G. Tajti, D.C.C. Wai, G. Panyi, R.S. Norton, The voltage-gated potassium channel KV1.3 as a therapeutic target for venom-derived peptides, Biochem. Pharmacol. 181 (2020) 114146, https://doi.org/10.1016/j.bcp.2020.114146.
[19] H. Wulff, P.A. Calabresi, R. Allie, S. Yun, M. Pennington, C. Beeton, K.G. Chandy, The voltage-gated Kv1.3 K(+) channel in effector memory T cells as new target for MS, J. Clin. Invest. 111 (11) (2003) 1703–1713.
[20] C. Beeton, H. Wulff, N.E. Standifer, P. Azam, K.M. Mullen, M.W. Pennington, A. Kolski-Andreaco, E. Wei, A. Grino, D.R. Counts, P.H. Wang, C.J. LeeHealey, B. S. Andrews, A. Sankaranarayanan, D. Homerick, W.W. Roeck, J. Tehranzadeh, K. L. Stanhope, P. Zimin, P.J. Havel, S. Griffey, H.-G. Knaus, G.T. Nepom, G. A. Gutman, P.A. Calabresi, K.G. Chandy, Kv1.3 channels are a therapeutic target for T cell-mediated autoimmune diseases, Proc. Natl. Acad. Sci. U. S. A. 103 (46) (2006) 17414–17419.
[21] C. Beeton, M.W. Pennington, H. Wulff, S. Singh, D. Nugent, G. Crossley, I. Khaytin, P.A. Calabresi, C.-Y. Chen, G.A. Gutman, K.G. Chandy, Targeting effector memory T cells with a selective peptide inhibitor of Kv1.3 channels for therapy of autoimmune diseases, Mol. Pharmacol. 67 (4) (2005) 1369–1381.
[22] G. Panyi, G. Vámosi, A. Bodnár, R. Gáspár, S. Damjanovich, Looking through ion channels: recharged concepts in T-cell signaling, Trends Immunol. 25 (11) (2004) 565–569.
[23] F. Papp, P. Hajdu, G. Tajti, A. Toth, E. Nagy, Z. Fazekas, S. Kovacs, G. Vámosi, Z. Varga, G. Panyi, Periodic Membrane Potential and Ca(2+) Oscillations in T Cells Forming an Immune Synapse, Int. J. Mol. Sci. 21 (5) (2020) 1568, https://doi.org/10.3390/ijms21051568.
[24] G. Panyi, L.D. Possani, R.C. Rodriguez de la Vega, R. Gaspar, Z. Varga, K+ channel blockers: novel tools to inhibit T cell activation leading to specific immunosuppression, Curr. Pharm. Des. 12 (18) (2006) 2199–2220.
[25] Z. Varga, G. Gurrola-Briones, F. Papp, R.C. Rodríguez de la Vega, G. Pedraza-Alva, R.B. Tajhya, R. Gaspar, L. Cardenas, Y. Rosenstein, C. Beeton, L.D. Possani, G. Panyi, Vm24, a natural immunosuppressive peptide, potently and selectively blocks Kv1.3 potassium channels of human T cells, Mol. Pharmacol. 82 (3) (2012) 372–382.
[26] G.B. Gurrola, R.A. Hernández-López, R.C. Rodríguez de la Vega, Z. Varga, C.V. F. Batista, S.P. Salas-Castillo, G. Panyi, F. del Río-Portilla, L.D. Possani, Structure, function, and chemical synthesis of Vaejovis mexicanus peptide 24: a novel potent blocker of Kv1.3 potassium channels of human T lymphocytes, Biochemistry 51 (19) (2012) 4049–4061.
[27] G. Tajti, T.G. Szanto, A. Csoti, G. Racz, C. Evaristo, P. Hajdu, G. Panyi, Immunomagnetic separation is a suitable method for electrophysiology and ion channel pharmacology studies on T cells, Channels (Austin) 15 (1) (2021) 53–66.
[28] M. Bagdany, C.V. Batista, N.A. Valdez-Cruz, S. Somodi, R.C. Rodriguez de la Vega, A.F. Licea, et al., Anuroctoxin, a new scorpion toxin of the alpha-KTx 6 subfamily, is highly selective for Kv1.3 over IKCa1 ion channels of human T lymphocytes, Mol. Pharmacol. 67 (4) (2005) 1034–1044.
[29] G. Corzo, F. Papp, Z. Varga, O. Barraza, P.G. Espino-Solis, R.C. Rodríguez de la Vega, R. Gaspar, G. Panyi, L.D. Possani, A selective blocker of Kv1.2 and Kv1.3 potassium channels from the venom of the scorpion Centruroides suffusus suffusus, Biochem. Pharmacol. 76 (9) (2008) 1142–1154.
[30] S. Grissmer, A.N. Nguyen, J. Aiyar, D.C. Hanson, R.J. Mather, G.A. Gutman, et al., Pharmacological characterization of five cloned voltage-gated K+ channels, types Kv1.1, 1.2, 1.3, 1.5, and 3.1, stably expressed in mammalian cell lines, Mol. Pharmacol. 45 (6) (1994) 1227–1234.
[31] M. Péter Jr., Z. Varga, P. Hajdu, R. Gáspár Jr., S. Damjanovich, E. Horjales, L. D. Possani, G. Panyi, Effects of toxins Pi2 and Pi3 on human T lymphocyte Kv1.3 channels: the role of Glu7 and Lys24, J Membr. Biol. 179 (1) (2001) 13–25.
[32] V. Avdonin, X.D. Tang, T. Hoshi, Stimulatory action of internal protons on Slo1 BK channels, Biophys. J. 84 (5) (2003) 2969–2980.
[33] S. Grissmer, A.N. Nguyen, M.D. Cahalan, Calcium-activated potassium channels in resting and activated human T lymphocytes. Expression levels, calcium dependence, ion selectivity, and pharmacology, J. Gen. Physiol. 102 (4) (1993) 601–630.
[34] A. Banerjee, A. Lee, E. Campbell, R. Mackinnon, Structure of a pore-blocking toxin in complex with a eukaryotic voltage-dependent K(+) channel, Elife 2 (2013) e00594.
[35] A.E. Leffler, A. Kuryatov, H.A. Zebroski, S.R. Powell, P. Filipenko, A.K. Hussein, J. Gorson, A. Heizmann, S. Lyskov, R.W. Tsien, S.F. Poget, A. Nicke, J. Lindstrom, B. Rudy, R. Bonneau, M. Holford, Discovery of peptide ligands through docking and virtual screening at nicotinic acetylcholine receptor homology models, Proc. Natl. Acad. Sci. U. S. A. 114 (38) (2017), https://doi.org/10.1073/pnas.1703952114.
[36] P. Liu, B. Kim, R.A. Friesner, B.J. Berne, Replica exchange with solute tempering: a method for sampling biological systems in explicit water, Proc. Natl. Acad. Sci. U. S. A. 102 (39) (2005) 13749–13754.
[37] L. Wang, R.A. Friesner, B.J. Berne, Replica exchange with solute scaling: a more efficient version of replica exchange with solute tempering (REST2), J. Phys. Chem. B 115 (30) (2011) 9431–9438.
[38] E. Harder, W. Damm, J. Maple, C. Wu, M. Reboul, J.Y. Xiang, L. Wang, D. Lupyan, M.K. Dahlgren, J.L. Knight, J.W. Kaus, D.S. Cerutti, G. Krilov, W.L. Jorgensen, R. Abel, R.A. Friesner, OPLS3: A Force Field Providing Broad Coverage of Drug-like Small Molecules and Proteins, J. Chem. Theory Comput. 12 (1) (2016) 281–296.
[39] J. Chrencik, C. Roth, M. Terakado, H. Kurata, R. Omi, Y. Kihara, D. Warshaviak, S. Nakade, G. Asmar-Rovira, M. Mileni, H. Mizuno, M. Griffith, C. Rodgers, G. Han, J. Velasquez, J. Chun, R. Stevens, M. Hanson, Crystal Structure of Antagonist Bound Human Lysophosphatidic Acid Receptor 1, Cell 161 (7) (2015) 1633–1643.
[40] V.R. Krishnamurthy, M.Y.R. Sardar, Y.u. Ying, X. Song, C. Haller, E. Dai, X. Wang, D. Hanjaya-Putra, L. Sun, V. Morikis, S.I. Simon, R.J. Woods, R.D. Cummings, E. L. Chaikof, Glycopeptide analogues of PSGL-1 inhibit P-selectin in vitro and in vivo, Nat. Commun. 6 (1) (2015), https://doi.org/10.1038/ncomms7387.
[41] S. Sirin, D.A. Pearlman, W. Sherman, Physics-based enzyme design: predicting binding affinity and catalytic activity, Proteins 82 (12) (2014) 3397–3409.
[42] P.A. Kollman, I. Massova, C. Reyes, B. Kuhn, S. Huo, L. Chong, et al., Calculating structures and free energies of complex molecules: combining molecular mechanics and continuum models, Acc. Chem. Res. 33 (12) (2000) 889–897.
[43] E. Wang, H. Sun, J. Wang, Z. Wang, H. Liu, J.Z.H. Zhang, T. Hou, End-Point Binding Free Energy Calculation with MM/PBSA and MM/GBSA: Strategies and Applications in Drug Design, Chem. Rev. 119 (16) (2019) 9478–9508.
[44] S. Genheden, U. Ryde, The MM/PBSA and MM/GBSA methods to estimate ligand-binding affinities, Expert Opin. Drug Discov. 10 (5) (2015) 449–461.

[45] H. Gohlke, C. Kiel, D.A. Case, Insights into protein-protein binding by binding free energy calculation and free energy decomposition for the Ras-Raf and Ras-RalGDS complexes, J. Mol. Biol. 330 (4) (2003) 891–913.
[46] M. Aldeghi, M.J. Bodkin, S. Knapp, P.C. Biggin, Statistical Analysis on the Performance of Molecular Mechanics Poisson-Boltzmann Surface Area versus Absolute Binding Free Energy Calculations: Bromodomains as a Case Study, J. Chem. Inf. Model. 57 (9) (2017) 2203–2221.
[47] S.A. Goldstein, C. Miller, Mechanism of charybdotoxin block of a voltage-gated K+ channel, Biophys. J. 65 (4) (1993) 1613–1619.
[48] A. Balajthy, S. Somodi, Z. Pethő, M. Péter, Z. Varga, G.P. Szabó, G. Paragh, L. Vígh, G. Panyi, P. Hajdu, 7DHC-induced changes of Kv1.3 operation contributes to modified T cell function in Smith-Lemli-Opitz syndrome, Pflugers Arch. 468 (8) (2016) 1403–1418.
[49] J.I. Veytia-Bucheli, J.M. Jiménez-Vargas, E.I. Melchy-Pérez, M.A. Sandoval-Hernández, L.D. Possani, Y. Rosenstein, Kv1.3 channel blockade with the Vm24 scorpion toxin attenuates the CD4(+) effector memory T cell response to TCR stimulation, Cell Commun. Signal. 16 (1) (2018), https://doi.org/10.1186/s12964-018-0257-7.
[50] O. Dobrovinskaya, I. Delgado-Enciso, L.J. Quintero-Castro, C. Best-Aguilera, R. M. Rojas-Sotelo, I. Pottosin, Placing ion channels into a signaling network of T cells: from maturing thymocytes to healthy T lymphocytes or leukemic T lymphoblasts, Biomed. Res. Int. 2015 (2015) 1–32.
[51] M. Dauplais, A. Lecoq, J. Song, J. Cotton, N. Jamin, B. Gilquin, C. Roumestand, C. Vita, C.C. de Medeiros, E.G. Rowan, A.L. Harvey, A. Ménez, On the convergent evolution of animal toxins. Conservation of a diad of functional residues in potassium channel-blocking toxins with unrelated structures, J. Biol. Chem. 272 (7) (1997) 4302–4309.
[52] S.A. Goldstein, D.J. Pheasant, C. Miller, The charybdotoxin receptor of a Shaker K+ channel: peptide and channel residues mediating molecular recognition, Neuron 12 (6) (1994) 1377–1388.
[53] O. Castañeda, V. Sotolongo, A.M. Amor, R. Stöcklin, A.J. Anderson, A.L. Harvey, Å. Engström, C. Wernstedt, E. Karlsson, Characterization of a potassium channel toxin from the Caribbean Sea anemone Stichodactyla helianthus, Toxicon 33 (5) (1995) 603–613.
[54] J.E. Tudor, P.K. Pallaghy, M.W. Pennington, R.S. Norton, Solution structure of ShK toxin, a novel potassium channel inhibitor from a sea anemone, Nat. Struct. Biol. 3 (4) (1996) 317–320.
[55] M. Garcia-Calvo, R.J. Leonard, J. Novick, S.P. Stevens, W. Schmalhofer, G. J. Kaczorowski, M.L. Garcia, Purification, characterization, and biosynthesis of margatoxin, a component of Centruroides margaritatus venom that selectively inhibits voltage-dependent potassium channels, J. Biol. Chem. 268 (25) (1993) 18866–18874.
[56] A. Bartok, A. Toth, S. Somodi, T.G. Szanto, P. Hajdu, G. Panyi, Z. Varga, Margatoxin is a non-selective inhibitor of human Kv1.3 K+ channels, Toxicon 87 (2014) 6–16.
[57] S. Mouhat, V. Visan, S. Ananthakrishnan, H. Wulff, N. Andreotti, S. Grissmer, et al., K+ channel types targeted by synthetic OSK1, a toxin from Orthochirus scrobiculosus scorpion venom, Biochem. J. 385 (Pt 1) (2005) 95–104.
[58] B. Lebrun, R. Romi-lebrun, M.-F. Martin-eauclaire, A. Yasuda, M. Ishiguro, Y. Oyama, O. Pongs, T. Nakajima, A four-disulphide-bridged toxin, with high affinity towards voltage-gated K+ channels, isolated from Heterometrus spinnifer (Scorpionidae) venom, Biochem. J. 328 (1) (1997) 321–327.
[59] F. Papp, C.V.F. Batista, Z. Varga, M. Herceg, S.A. Román-González, R. Gaspar, L. D. Possani, G. Panyi, Tst26, a novel peptide blocker of Kv1.2 and Kv1.3 channels from the venom of Tityus stigmurus, Toxicon 54 (4) (2009) 379–389.
[60] M.H. Rashid, R. Huq, M.R. Tanner, S. Chhabra, K.K. Khoo, R. Estrada, V. Dhawan, S. Chauhan, M.W. Pennington, C. Beeton, S. Kuyucak, R.S. Norton, A potent and Kv1.3-selective analogue of the scorpion toxin HsTX1 as a potential therapeutic for autoimmune diseases, Sci. Rep. 4 (1) (2015), https://doi.org/10.1038/srep04509.
[61] B. Gilquin, S. Braud, M.A.L. Eriksson, B. Roux, T.D. Bailey, B.T. Priest, M.L. Garcia, A. Ménez, S. Gasparini, A variable residue in the pore of Kv1 channels is critical for the high affinity of blockers from sea anemones and scorpions, J. Biol. Chem. 280 (29) (2005) 27093–27102.
[62] A. Bartok, K. Fehér, A. Bodor, K. Rákosi, G.K. Tóth, K.E. Kövér, G. Panyi, Z. Varga, An engineered scorpion toxin analogue with improved Kv1.3 selectivity displays reduced conformational flexibility, Sci. Rep. 5 (1) (2016), https://doi.org/10.1038/srep18397.
[63] B. Shen, Z. Cao, W. Li, J.-M. Sabatier, Y. Wu, Treating autoimmune disorders with venom-derived peptides, Expert Opin. Biol. Ther. 17 (9) (2017) 1065–1075.
[64] Š. Gubič, L.A. Hendrickx, Ž. Toplak, M. Sterle, S. Peigneur, T. Tomašič, L.A. Pardo, J. Tytgat, A. Zega, L.P. Mašič, Discovery of KV 1.3 ion channel inhibitors: Medicinal chemistry approaches and challenges, Med. Res. Rev. 41 (4) (2021) 2423–2473.
[65] K. Kalman, M.W. Pennington, M.D. Lanigan, A. Nguyen, H. Rauer, V. Mahnir, K. Paschetto, W.R. Kem, S. Grissmer, G.A. Gutman, E.P. Christian, M.D. Cahalan, R. S. Norton, K.G. Chandy, ShK-Dap22, a potent Kv1.3-specific immunosuppressive polypeptide, J. Biol. Chem. 273 (49) (1998) 32697–32707.
[66] S. Mouhat, G. Teodorescu, D. Homerick, V. Visan, H. Wulff, Y. Wu, S. Grissmer, H. Darbon, M. De Waard, J.-M. Sabatier, Pharmacological profiling of Orthochirus scrobiculosus toxin 1 analogs with a trimmed N-terminal domain, Mol. Pharmacol. 69 (1) (2006) 354–362.
[67] Z. Chen, Y. Hu, J. Hu, W. Yang, J.-M. Sabatier, M. De Waard, Z. Cao, W. Li, S. Han, Y. Wu, Unusual binding mode of scorpion toxin BmKTX onto potassium channels relies on its distribution of acidic residues, Biochem. Biophys. Res. Commun. 447 (1) (2014) 70–76.
[68] K.M. Giangiacomo, Y. Ceralde, T.J. Mullmann, Molecular basis of alpha-KTx specificity, Toxicon 43 (8) (2004) 877–886.
[69] S. Han, H. Yi, S.-J. Yin, Z.-Y. Chen, H. Liu, Z.-J. Cao, Y.-L. Wu, W.-X. Li, Structural basis of a potent peptide inhibitor designed for Kv1.3 channel, a therapeutic target of autoimmune disease, J. Biol. Chem. 283 (27) (2008) 19058–19065.
[70] M. Pennington, S. Chang, S. Chauhan, R. Huq, R. Tajhya, S. Chhabra, R. Norton, C. Beeton, Development of highly selective Kv1.3-blocking peptides based on the sea anemone peptide ShK, Mar. Drugs 13 (1) (2015) 529–542.
[71] U. Schönbeck, F. Mach, P. Libby, CD154 (CD40 ligand), Int. J. Biochem. Cell. Biol. 32 (7) (2000) 687–693.
[72] A.A. Chimote, P. Hajdu, A.M. Sfyris, B.N. Gleich, T. Wise-Draper, K.A. Casper, L. Conforti, Kv1.3 Channels Mark Functionally Competent CD8+ Tumor-Infiltrating Lymphocytes in Head and Neck Cancer, Cancer Res. 77 (1) (2017) 53–61.
[73] S. Feske, H. Wulff, E.Y. Skolnik, Ion channels in innate and adaptive immunity, Annu. Rev. Immunol. 33 (1) (2015) 291–353.
[74] C. Beeton, H. Wulff, J. Barbaria, O. Clot-Faybesse, M. Pennington, D. Bernard, M. D. Cahalan, K.G. Chandy, E. Béraud, Selective blockade of T lymphocyte K(+) channels ameliorates experimental autoimmune encephalomyelitis, a model for multiple sclerosis, Proc. Natl. Acad. Sci. U. S. A. 98 (24) (2001) 13942–13947.
[75] I.S. Oliveira, I.G. Ferreira, G.M. Alexandre-Silva, F.A. Cerni, C.M. Cremonez, E. C. Arantes, U. Zottich, M.B. Pucca, Scorpion toxins targeting Kv1.3 channels: insights into immunosuppression, J. Venom. Anim. Toxins Incl. Trop. Dis. 25 (2019), https://doi.org/10.1590/1678-9199-jvatitd-1481-18.